

# Asymmetry in summertime atmospheric circulation anomalies over the northwest Pacific during decaying phase of El Niño and La Niña

Weichen Tao<sup>1,4</sup> · Gang Huang<sup>1,2</sup> · Renguang Wu<sup>1,3</sup> · Kaiming Hu<sup>1,2,3</sup> · Pengfei Wang<sup>1,3</sup> · Dong Chen<sup>5</sup>

Received: 26 January 2016 / Accepted: 30 October 2016 / Published online: 8 November 2016  
© Springer-Verlag Berlin Heidelberg 2016

**Abstract** The present study has revealed the asymmetric characteristics of summertime atmospheric circulation anomalies over the Indo-Pacific for El Niño and La Niña, as well as the possible mechanism. During the summer when El Niño has dissipated, there are basin-wide warming over the tropical Indian Ocean (TIO) and cooling over the equatorial central and eastern Pacific (CEP). The northwest Pacific (NWP) anticyclone is maintained by a combined effect of the TIO warming and equatorial CEP cooling. The impact of TIO warming is via the Kelvin wave-induced divergence mechanism, and the effect of CEP cooling is by stimulating a Rossby wave response to its northwest. Correspondingly, there are lower (upper) level convergence (divergence) over the TIO and divergence (convergence) over the NWP. The tropical atmospheric waves and large-scale circulation anomalies could couple together and maintain the anticyclone. However, for La Niña, there are easterly wind anomalies over the equatorial western Pacific, and the anomalous NWP cyclone (NWPC) is weak

and shifts northwestward, which are largely different from El Niño. The equatorial CEP cooling plays a dominant role in the maintenance of NWPC. The negative rainfall anomalies induced by CEP cooling force the anticyclonic wind anomalies over the WP as a Rossby wave response, which further cause the lower (upper) level convergence (divergence) over the MC and NWP. The resultant convergence leads to the enhanced convection there, inducing the NWPC as a Rossby wave response. Besides, the equatorial easterly wind anomalies trigger the upwelling oceanic Kelvin wave and maintain the CEP cooling as the Bjerknes feedback.

**Keywords** Asymmetry · ENSO · El Niño and La Niña · Northwest Pacific circulation · Central and eastern Pacific cooling

## 1 Introduction

El Niño-Southern Oscillation (ENSO) is a dominant inter-annual variability over the tropical Pacific and exerts the great influence on global climate through atmospheric teleconnections (e.g., Lau and Nath 1996; Trenberth et al. 1998; Webster et al. 1998). It contains two phases, the warm phase (El Niño) and the cold phase (La Niña). However, El Niño and La Niña are not simply mirror images, but have significant asymmetry in spatial structure (e.g., Hoerling et al. 1997; Burgers and Stephenson 1999; Kang and Kug 2002; Jin et al. 2003; An and Jin 2004; McPhaden and Zhang 2009; Su et al. 2010) and duration (e.g., Okumura and Deser 2010; Okumura et al. 2011; Hu et al. 2013).

ENSO is a major factor for the East Asian climate variability. The warming (cooling) over the equatorial eastern

✉ Gang Huang  
hg@mail.iap.ac.cn

<sup>1</sup> State Key Laboratory of Numerical Modeling for Atmospheric Sciences and Geophysical Fluid Dynamics, Institute of Atmospheric Physics, Chinese Academy of Sciences, Beijing 100029, China

<sup>2</sup> Joint Center for Global Change Studies, Beijing 100875, China

<sup>3</sup> Center for Monsoon System Research, Institute of Atmospheric Physics, Chinese Academy of Sciences, Beijing 100029, China

<sup>4</sup> University of Chinese Academy of Sciences, Beijing 100049, China

<sup>5</sup> Chengdu University of Information Technology, Chengdu 610225, China

Pacific suppresses (enhances) convection over the western Pacific (WP), which affects the variability of East Asian monsoon (Huang and Wu 1989; Huang and Sun 1992; Zhang et al. 1996). The anomalous atmospheric circulation over the northwest Pacific (NWP) plays an important role in bridging teleconnection from ENSO to the East Asian climate (Zhang et al. 1996; Chang et al. 2000a, b; Wang et al. 2000; Wu et al. 2003; Yang et al. 2007; Xie et al. 2009; Chen et al. 2012, 2014; Wang and Wu 2012). The anomalous NWP anticyclone/cyclone (NWPAC/NWPC) would weaken/intensify the East Asian monsoon. The NWP circulation anomalies develop rapidly in late fall of the year when ENSO matures (Wang et al. 2000), and the anomalies can persist into summer (e.g., Wu et al. 2003; Yang et al. 2007; Xie et al. 2009; Tao et al. 2015). There are two possible mechanisms maintaining the NWPAC during the different phases of El Niño: (1) From fall to spring, the NWPAC is a Rossby wave response to SST cooling located to its southeast. The northeasterly wind anomalies of NWPAC superimpose on the northeasterly trade winds, and reinforce initial cold SST anomalies via evaporation, forming a positive feedback between SST and circulation anomalies (Wang et al. 2000; Wang and Zhang 2002). (2) During summer when El Niño has dissipated, the tropical Indian Ocean (TIO) warming prolongs the influence of El Niño, which contributes to the development of NWPAC via the “capacitor effect” (Yang et al. 2007, 2010; Wu et al. 2009a; Xie et al. 2009).

The atmospheric response to El Niño and La Niña is also nonlinear (Hoerling et al. 1997) though most studies use the linear statistical methods, such as empirical orthogonal function (EOF), regression or correlation to analyze atmospheric circulation anomalies associated with ENSO. Several studies have investigated the asymmetry of atmospheric response to ENSO over East Asia. For El Niño, there are southerly wind anomalies along the coast of East Asia. However, the opposite meridional wind anomalies do not appear during La Niña, and the impact of La Niña on the East Asian monsoon seems weaker than El Niño (Zhang et al. 1996). Wu et al. (2010b) studied the asymmetry of NWP lower level circulation anomalies in boreal winter, which are weaker and shift more westward during La Niña than El Niño. They interpreted that both the asymmetry of anomalous heating and NWP sea surface temperature (SST) anomalies contribute to this asymmetric response. Zhang et al. (2014) further revealed that the asymmetric response of atmospheric circulation is related to the intra-seasonal oscillation, leading to the asymmetry of rainfall anomalies over southern China during boreal winter.

Until now most studies focused on the East Asian winter monsoon (EAWM) in the mature phase of ENSO, and the asymmetric characteristics of East Asian summer monsoon (EASM) in the decaying phase of ENSO are still not clear.

Thus, we attempt to address the following questions in present study. First, is the summertime atmospheric response over the NWP between El Niño and La Niña asymmetric? Second, if so, what is the physical mechanism causing the asymmetry? The rest of the paper is organized as follows. Section 2 describes the data and analysis methods. The asymmetric characteristics, including the SST, precipitation and circulation anomalies, are examined in Sect. 3. Section 4 evaluates the possible mechanism, which are further explored by using the results of an atmospheric general circulation model (AGCM) and a Linear Baroclinic Model (LBM) in Sect. 5. Section 6 provides the summary.

## 2 Data and analysis methods

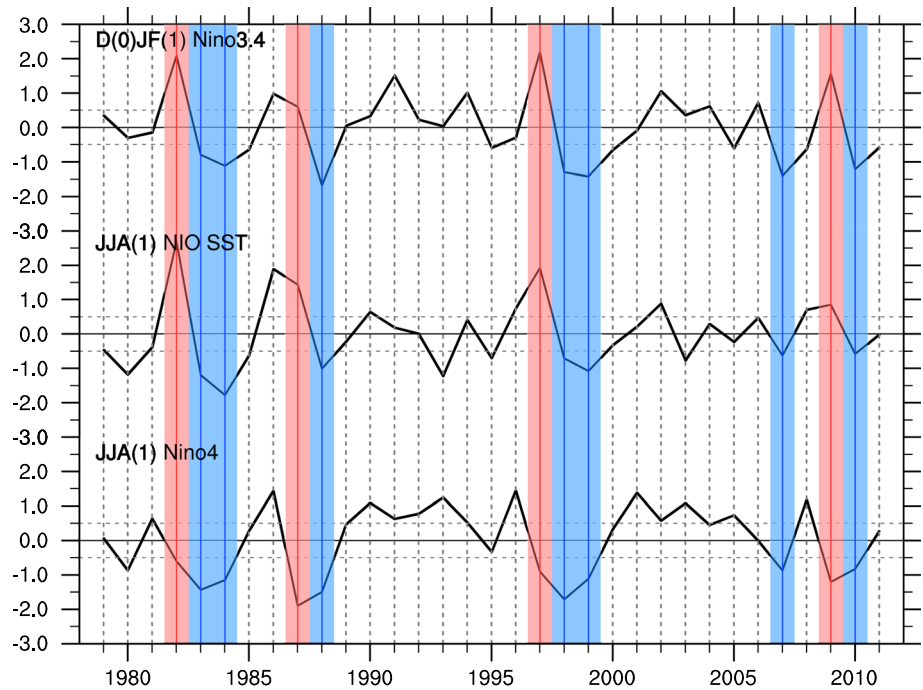
### 2.1 Data

The SST data used in present study is the Hadley Centre Sea ICE and Sea Surface Temperature (HadISST) dataset (Rayner et al. 2003). It has a  $1^\circ \times 1^\circ$  horizontal resolution and starts from January 1870 to the present. The monthly mean atmospheric variables used here are the National Centers for Environmental Prediction/National Center for Atmospheric Research (NCEP/NCAR) reanalysis product (Kalnay et al. 1996), spanning the period from January 1948 to the present. This dataset is available in a  $2.5^\circ \times 2.5^\circ$  horizontal resolution and extends from 1000 to 10 hPa with 17 pressure levels in vertical. The precipitation data from the monthly mean Global Precipitation Climatology Project (GPCP; Adler et al. 2003), which has a  $2.5^\circ \times 2.5^\circ$  horizontal resolution since January 1979, is also used. Due to the decadal shift in El Niño influences on Indo-Western Pacific and East Asian climate in the 1970s (Wang 1995; Wang et al. 2008; Huang et al. 2010; Xie et al. 2010; Wu et al. 2012), the period of above data are selected from January 1979 to December 2012.

### 2.2 Analysis methods

The monthly mean climatology is first calculated for the study period, and interannual anomalies are then computed as the departure from the climatology. In this study, we focus on the interannual relationship, and the linear trend has been removed from all the data. Hereafter, any month in the El Niño onset and decay year is identified by suffix (0) and (1), respectively. DJF represents the seasonal mean in December–January–February, MAM represents the seasonal mean in March–April–May, and JJA represents the seasonal mean in June–July–August. The intensity of NWP circulation anomalies is defined as the difference of 850 hPa zonal winds between a southern region ( $5^\circ$ – $15^\circ$ N,  $90^\circ$ – $130^\circ$ E) and a northern region ( $22.5^\circ$ – $32.5^\circ$ N,

**Fig. 1** The evolution of the normalized Niño3.4 index (*top*) during D(0)JF(1), NIO SST anomalies (*middle*) during JJA(1) and Niño4 index (*bottom*) during JJA(1) from 1979 to 2011. NIO SST anomalies and Niño4 index are pushed forward for a year. According to the definitions in Table 1, a total of 4 El Niño events (*red shaded* 1982, 1987, 1997, 2009), 7 La Niña events (*blue shaded* 1983, 1984, 1988, 1998, 1999, 2007, 2010) are identified



110°–140°E), following Wang and Fan (1999). The Niño3.4 index is defined as SST anomalies averaged over the central and eastern equatorial Pacific (CEP, 5°S–5°N, 170°–120°W), and the Niño4 index is defined as SST anomalies averaged over the equatorial central Pacific (CP, 5°S–5°N, 160°E–150°W). The domain of north Indian Ocean (NIO) is defined as 0°–20°N, 40°–100°E.

To diagnose the contribution of the factors (e.g., circulation and moisture) to moisture transportation, moisture budget is analyzed in the present study. The moisture transportation can be decomposed:

$$\begin{aligned} \langle -\nabla \cdot (qV)' \rangle &= \langle -(q\nabla \cdot V)' \rangle + \langle -(V \cdot \nabla q)' \rangle \\ &= \langle -\bar{\omega} \partial_p q' \rangle + \langle -\omega' \partial_p \bar{q} \rangle + \langle -\omega' \partial_p q' \rangle + \langle -\bar{V} \cdot \nabla q' \rangle \\ &\quad + \langle -V' \cdot \nabla \bar{q} + -V' \cdot \nabla q' \rangle \end{aligned}$$

where the variable with bar means climatology state, and the variable with prime mean the departure from the climatology state.  $q, V, \omega$  represent the specific humidity, horizontal wind, and pressure velocity, respectively. The value in angle bracket means a mass integration from the surface to 300 hPa, that is:

$$X = -\frac{1}{g} \int_{surface}^{300 \text{ hPa}} X dp$$

According to Yanai et al. (1973), the atmospheric apparent heat source  $Q_1$  is used to represent the total diabatic heating (including radiation, latent heating, and surface heat flux),

$$Q_1 = C_p \frac{\partial T}{\partial t} - C_p (\omega \sigma - \vec{V} \cdot \nabla T),$$

where  $C_p$  is the specific heat at constant pressure,  $T$  is the temperature,  $t$  is the time,  $\omega$  is the vertical p velocity,  $\sigma = RT/C_p P - \partial T/\partial P$  is the static stability,  $R$  is the gas constant,  $P$  is the pressure, and  $\vec{V}$  is the horizontal velocity vector.

Composite analysis is used, and the significance level is estimated based on the standard two-tailed Student’s  $t$  test. The normalized D(0)JF(1) Niño3.4 index, JJA(1) NIO SST index and Niño4 index shown in Fig. 1 are used to identify El Niño and La Niña events in this study. As mentioned before, the TIO warming persists into summer and unleash its influence when El Niño has dissipated (Yang et al. 2007, 2010; Wu et al. 2009a; Xie et al. 2009). Sometimes, El Niño decays rapidly into La Niña, and the CEP cooling could play a role in development and maintenance of the summertime NWPAC (Fan et al. 2013; Wang et al. 2013; Xiang et al. 2013; Chen et al. 2015). Thus, an El Niño event is firstly defined as normalized D(0)JF(1) Niño3.4 index is above 0.5. Then normalized JJA(1) NIO SST index requires more than 0.5 to emphasize the “capacitor effect”. Furthermore, normalized JJA(1) Niño4 index is below 0.5, indicating the decaying of CEP warming. El Niño tends to decay rapidly after the mature phase, whereas La Niña persists and re-emerges in the subsequent year (Kessler 2002; Larkin and Harrison 2002; McPhaden and Zhang 2009; Hu et al. 2013). Thus, a La Niña event is defined as normalized D(0)JF(1) Niño3.4 index is below -0.5, normalized JJA(1) NIO SST index and Niño4 index

**Table 1** The definitions of El Niño and La Niña, and the corresponding selected years for the period of 1979–2011

| Types   | Definitions  | Years                                    |
|---------|--|--|
| El Niño | Nor D(0)JF(1) Niño 3.4 > 0.5<br>Nor JJA(1) NIO > 0.5<br>Nor JJA(1) Niño 4 < 0.5    | 1982, 1987, 1997, 2009                   |
| La Niña | Nor D(0)JF(1) Niño 3.4 < -0.5<br>Nor JJA(1) NIO < -0.5<br>Nor JJA(1) Niño 4 < -0.5 | 1983, 1984, 1988, 1998, 1999, 2007, 2010 |

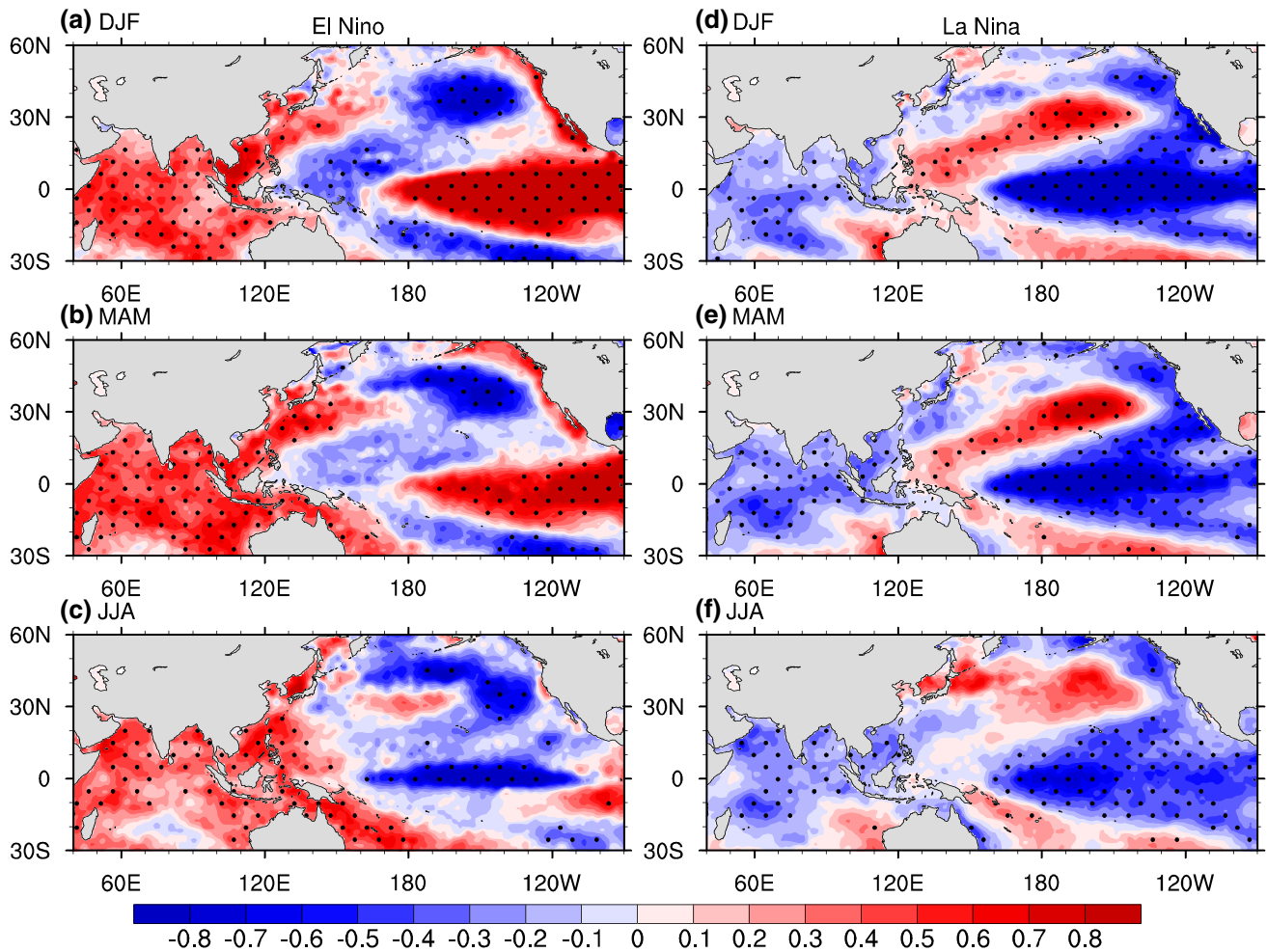


**Fig. 2** Composite anomalies of SST (°C) during D(0)JF(1), MAM(1) and JJA(1) for El Niño (left panels a–c) and La Niña (right panels d–f). Dots indicate significant level reaches 90%

are below  $-0.5$ . As a result, there are 4 El Niño events (1982, 1987, 1997 and 2009) and 7 La Niña events (1983, 1984, 1988, 1998, 1999, 2007 and 2010), which are listed in Table 1. Note that using all El Niño and La Niña events according to the 0.5 criterion does not alter the major conclusions, but the composite maps show weak intensity and less significance (figures not shown). The selected El Niño and La Niña events are more proper to present the asymmetric characteristics.

### 3 Observed asymmetric characteristics

#### 3.1 SST pattern

Figure 2 shows the evolution of SST anomalies for El Niño and La Niña from D(0)JF(1) to JJA(1). For El Niño, there exists significant SST warming in the equatorial CEP and TIO during D(0)JF(1) (Fig. 2a). From MAM(1) to JJA(1), the SST anomalies over the equatorial CEP decay rapidly, but the TIO

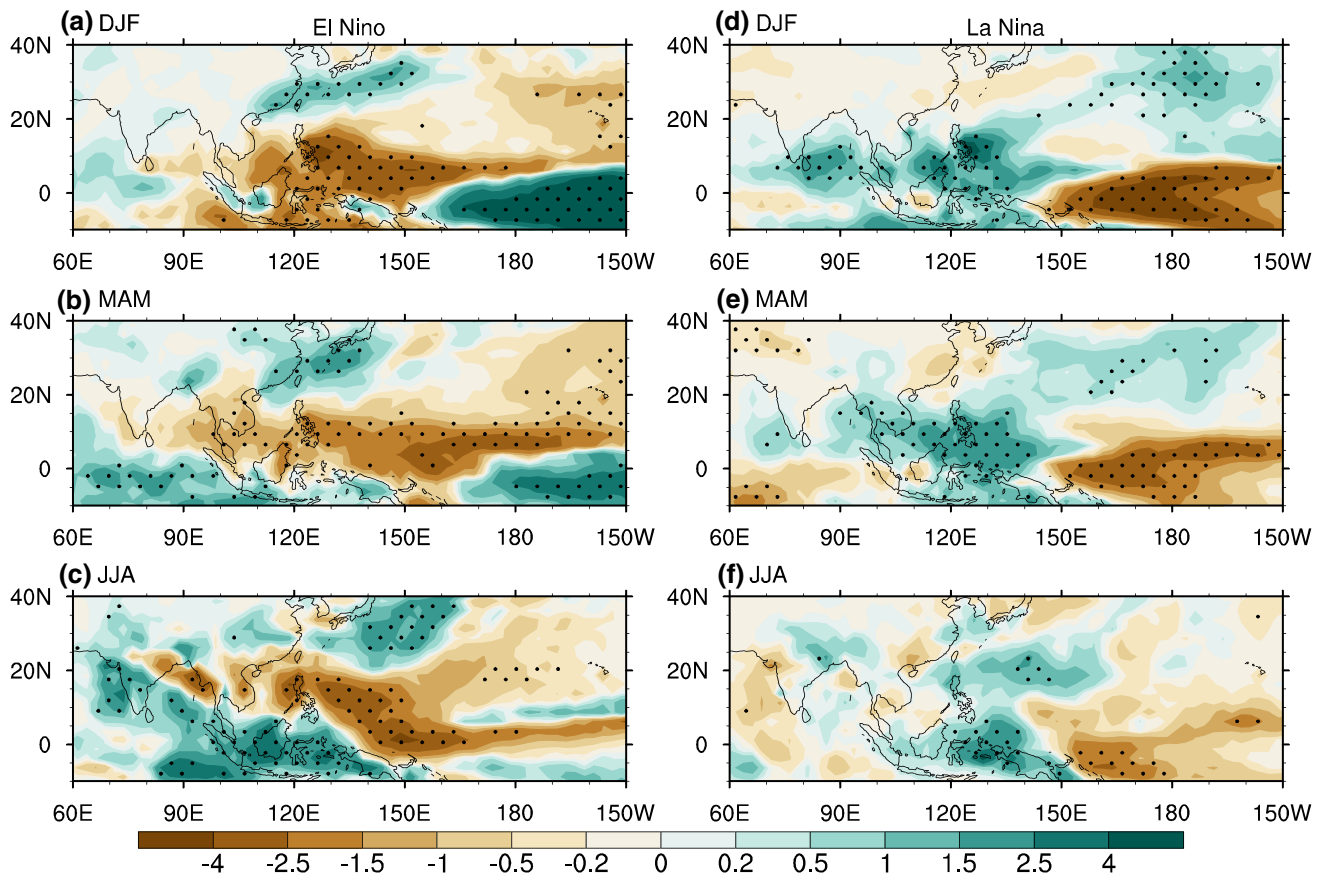


**Fig. 3** Composite anomalies of precipitation (mm) during D(0)JF(1), MAM(1) and JJA(1) for El Niño (left panels a–c) and La Niña (right panels d–f). Dots indicate significant level reaches 90%

warming sustains (Fig. 2b, c). Previous studies have revealed that El Niño is a major forcing for the TIO warming (Lau and Nath 1996; Klein et al. 1999; Xie et al. 2002; Wu et al. 2008; Du et al. 2009; Tao et al. 2014). Note that the negative SST anomalies tend to develop over the equatorial CEP during JJA(1) after the El Niño event, indicating the phase transition of ENSO. However, the La Niña-related SST anomalies are different from El Niño. The equatorial CEP cooling decays slowly and there are still significant SST anomalies during JJA(1) (Fig. 2d–f). Besides, the TIO SST anomalies do not show the basin-wide characteristic, and there is pronounced warming near the northwest coast of Australia. The similar Indo-Pacific pattern is also shown in CMIP5 models, which is caused by the westward bias in the simulation of ENSO's SST pattern (Tao et al. 2015). Okumura and Deser (2010) found that the coastal warming is induced by the northwesterly wind anomalies, which is attributed to the asymmetry of atmospheric response to El Niño and La Niña.

### 3.2 Indo-Pacific precipitation

Figure 3 shows the evolution of precipitation anomalies over the Indo-Pacific for El Niño and La Niña from D(0)

JF(1) to JJA(1). In D(0)JF(1), the large-scale suppressed rainfall anomalies are located over the Maritime Continent (MC) while enhanced rainfall anomalies are found over the equatorial CP for El Niño (Fig. 3a). Both the suppressed and enhanced rainfall anomalies decay rapidly in MAM(1) (Fig. 3b). The wet anomalies over the CP dissipate during JJA season, and the center of dry anomalies moves northeastward to the NWP (Fig. 3c). Note that the wet anomalies forced by TIO warming play a crucial role in the development of NWP dry anomalies through the Kelvin wave-induced Ekman divergence mechanism (Xie et al. 2009). For La Niña, the patterns of rainfall anomalies are almost opposite to El Niño during DJF and MAM season (Fig. 3a, b, d, e), but the centers shift more westward, which have been mentioned by Hoerling et al. (1997). In JJA(1), there exists considerable difference between El Niño and La Niña. The dry anomalies over the CP corresponding with equatorial CEP cooling persist through JJA, and there are no significant rainfall anomalies over the east Indian Ocean (Fig. 3f). Unlike the rainfall anomalies over the NWP with large zonal coverage for El Niño, the La Niña-related wet anomalies show large meridional coverage with two rainfall centers over the MC and NWP.

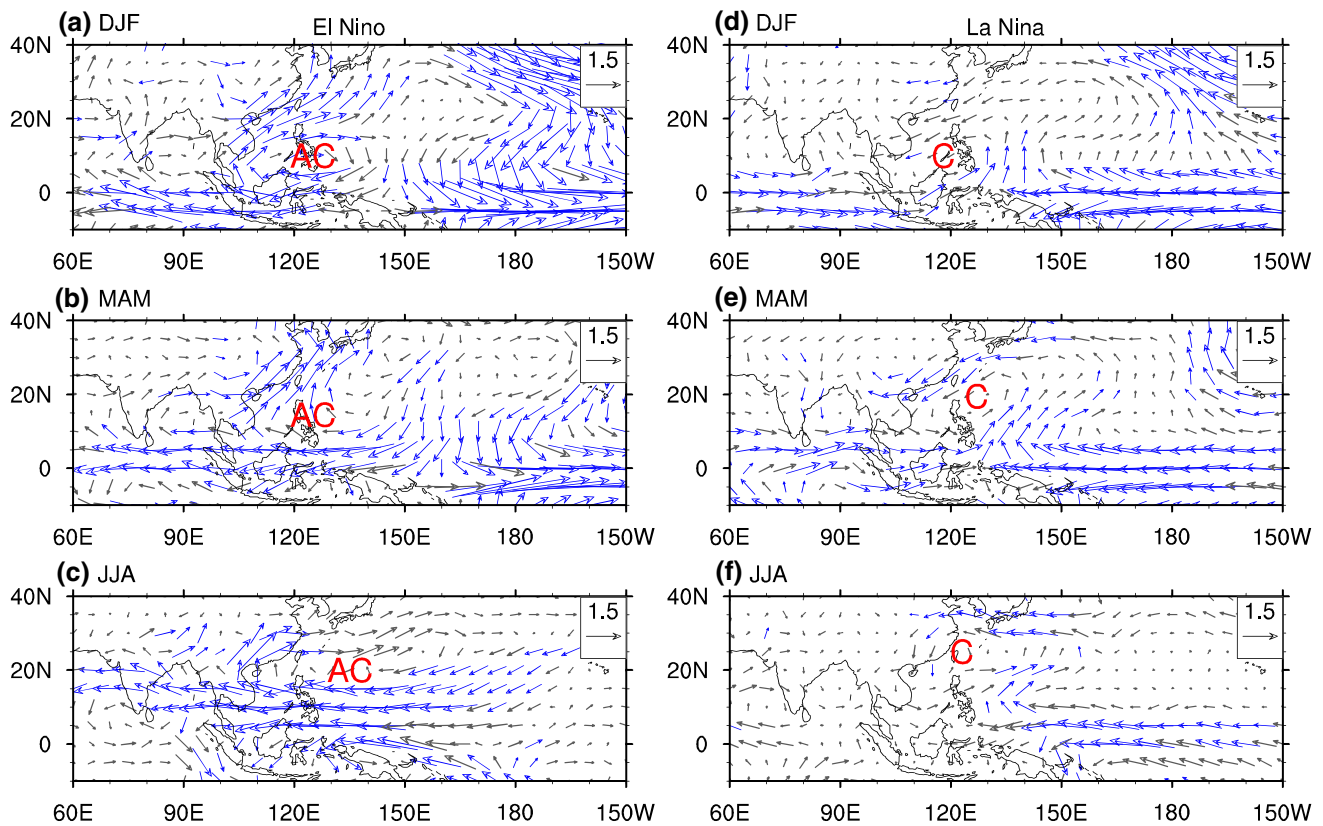


**Fig. 4** Composite anomalies of 850 hPa wind velocity ( $\text{m s}^{-1}$ ) during D(0)JF(1), MAM(1) and JJA(1) for El Niño (left panels a–c) and La Niña (right panels d–f). Blue vectors indicate significant level reaches

90%. ‘AC’ and ‘C’ represent the centers of anomalous NWPAC and NWPC, respectively

The wet and dry anomalies over the MC and CP present a zonal dipole pattern. The Indo-Pacific rainfall anomalies in JJA(1) for El Niño and La Niña are induced by the different SST patterns there, which is also emphasized by Lu and Lu (2014). Besides, as shown in Fig. 5 of Xie et al. (2009), the ENSO-related rainfall anomalies are mainly concentrated over the west Indian Ocean and there are no significant rainfall anomalies over the east Indian Ocean. Here, the asymmetry of TIO rainfall responses to El Niño and La Niña may explain this phenomenon.

### 3.3 Anomalous NWP circulation

The evolution of NWP circulation anomalies for El Niño and La Niña from D(0)JF(1) to JJA(1) are shown in Fig. 4. Large wind anomalies are observed over the NWP, and the NWPAC or NWPC moves northward in JJA(1). The asymmetry of NWP circulation anomalies in boreal winter and its influence on the EAWM have been investigated in previous studies (Wu et al. 2010b; Zhang et al. 2014). Thus, we pay more attention on the JJA season. For El Niño and La Niña, their corresponding lower level circulation anomalies are not symmetric (Fig. 4c, f). The center of NWPC for La

Niña is closer to the coast of East Asia, and its extent is smaller than El Niño (Fig. 4f). The intensity of NWP circulation anomalies for each event is further checked in Fig. 5. All El Niño events correspond to the NWPAC (Fig. 5a), and most La Niña events correspond to the NWPC except for the 2007 event (Fig. 5d). Most La Niña-related NWPCs are weaker than El Niño-related NWPACs, even with anomalous anticyclones after the 2007 event, which is due to that the location of circulation anomalies shifts more northward. Note that the anomalous NWPCs are stronger for 1983 and 1984 events, which will be discussed in the last section.

## 4 Possible mechanism

NWP circulation is sensitive to the tropical ocean status, and there are two views to understand the dynamic process. On one hand, tropical SST anomalies would lead to the adjustment of large-scale tropical circulation, including Walker and Hadley circulation, which in turn induces anomalous NWP circulation (Wu et al. 2009a, b; Chung et al. 2011; Chen and Zhou 2014). On the other hand, the

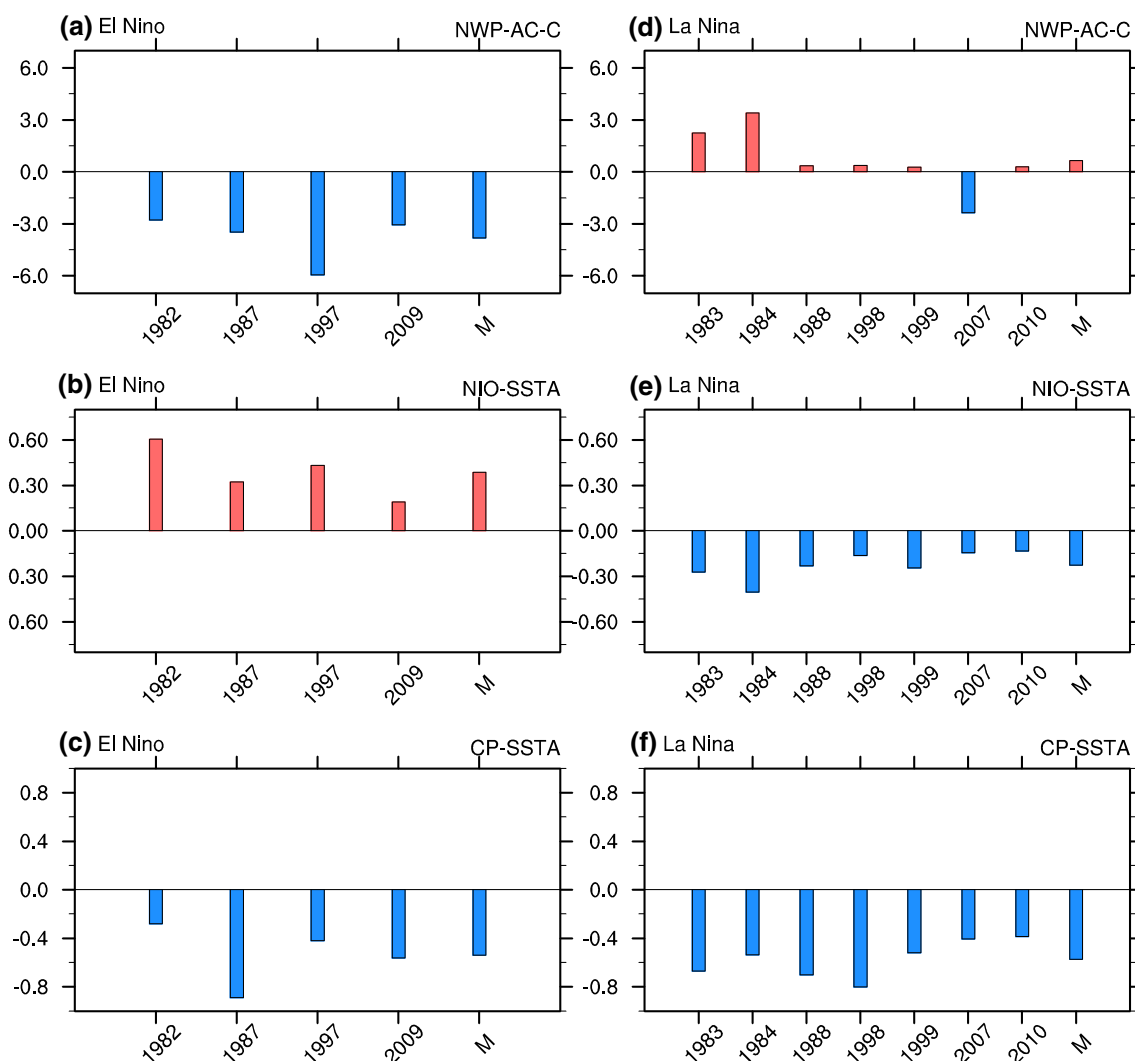


**Fig. 5** The intensity of NWP circulation anomalies, NIO and equatorial CP SST anomalies for El Niño (*left panels a–c*) and La Niña (*right panels d–f*). The *abscissa* represents the contained events

(numbers) and their corresponding composite mean (“M”) in each type. The *ordinate* represents the intensity of anomalies

lower level NWP circulation is sensitive to anomalous heating in atmosphere following Gill-response mechanism (Gill 1980; Wang et al. 2000; Xie et al. 2009; Fan et al. 2013; Karori et al. 2013; Chen et al. 2015). Thus, according to the asymmetric characteristics in the previous section, the possible mechanisms are analyzed in this section in order to investigate how these two aspects work together during JJA(1) in El Niño and La Niña. Besides, to better understand the dynamical processes in the rainfall response, moisture budget analysis is also performed.

#### 4.1 Kelvin wave-induced divergence for El Niño

During JJA season, the SST anomalies over the NWP have almost dissipated (Fig. 2c, f). So local air-sea interaction has little effect on the rainfall anomalies there, which seem

to be mainly forced by the remote oceans. Figure 6 shows the 1000–200 hPa mean tropospheric temperature (TT) and 200 hPa wind anomalies during JJA(1) for El Niño and La Niña. Due to the wet anomalies related to TIO warming (Fig. 3c), the TT anomalies over the TIO display the Matsuno-Gill (Matsuno 1966; Gill 1980) pattern with the warm Kelvin wave eastward to the equatorial WP for El Niño. Upper level southwesterly wind anomalies dominate the MC region (Fig. 6a), and lower level northeasterly wind anomalies are induced at the north flank of the Kelvin wave owing to the Ekman divergence (Fig. 4c). Then the resultant divergence over the NWP further trigger the suppressed convection there, inducing the anomalous anticyclone as the Rossby wave response (Xie et al. 2009). Correspondingly, there are lower (upper) level convergence (divergence) over the TIO and divergence (convergence) over the NWP (Fig. 7a, c).

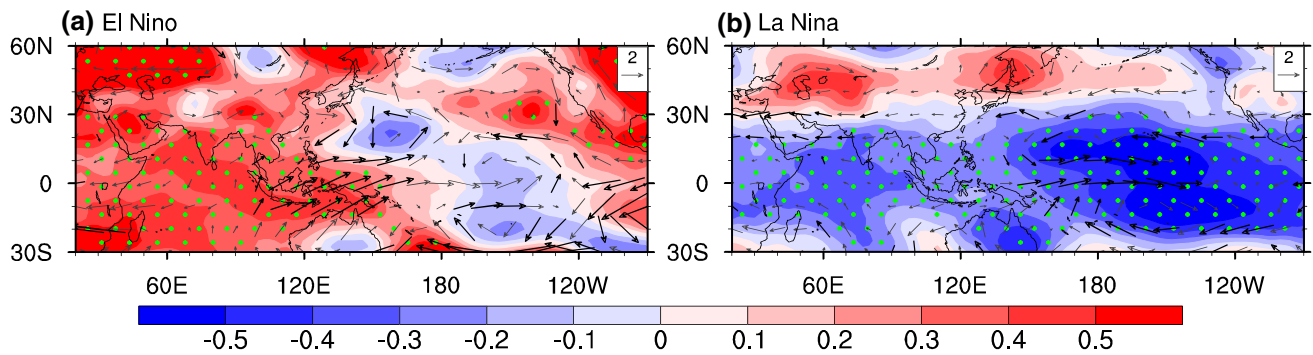


**Fig. 6** Composite anomalies of 1000–200 hPa mean tropospheric temperature (shaded °C) and 200 hPa wind velocity (vector  $\text{m s}^{-1}$ ) during JJA(1) for **a** El Niño and **b** La Niña. Green dots and black vec-

tors indicate significant level of tropospheric temperature and wind velocity reaches 90%, respectively

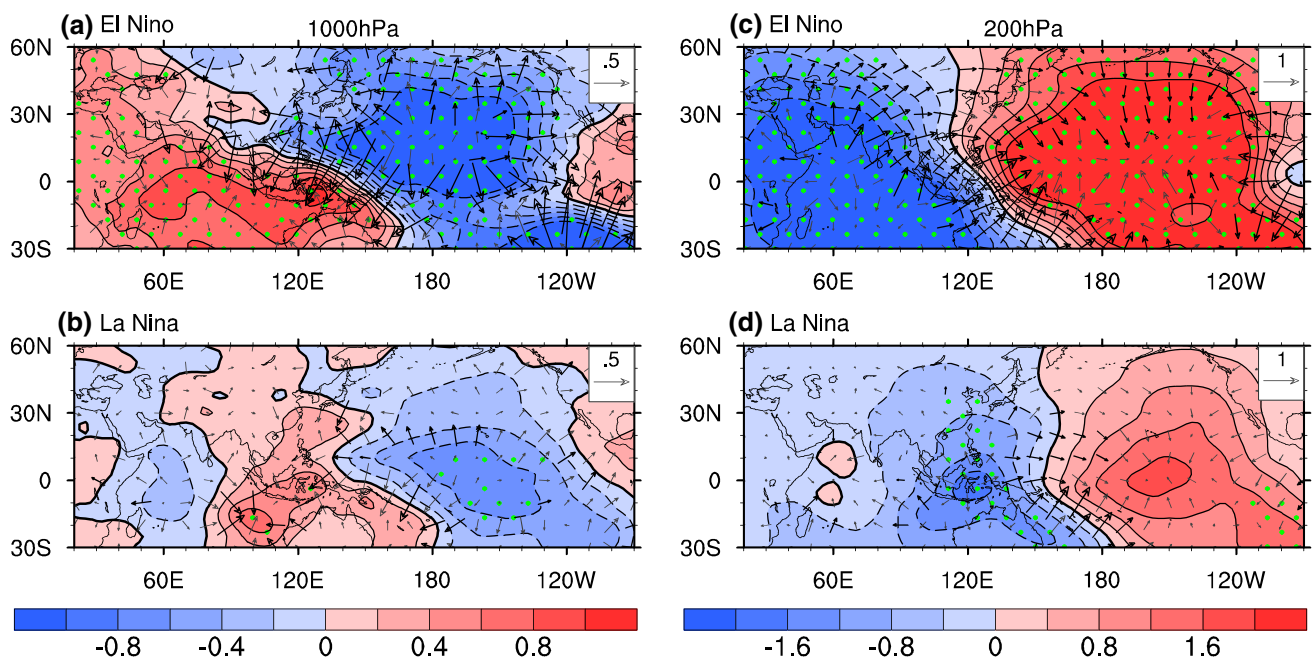


**Fig. 7** Composite anomalies of 1000 hPa (contour  $\text{CI} = 2 \times 10^5 \text{ m}^2 \text{ s}^{-1}$ ), 200 hPa potential velocity (contour  $\text{CI} = 4 \times 10^5 \text{ m}^2 \text{ s}^{-1}$ ) and relevant divergent wind component (vector  $\text{m s}^{-1}$ ) during JJA(1) for El Niño (top panels **a**, **c**) and La Niña

(bottom panels **b**, **d**). Green dots and black vectors indicate significant level of potential velocity and divergent wind component reaches 90%, respectively. Thick black lines indicate zero contour

To verify the relative contribution of circulation and moisture to the rainfall response over the NWP, moisture budget analysis is performed. The detailed information of the moisture budget equation is introduced in Sect. 2.2. Figure 8a–c presents the composite anomalies of column-integrated moisture flux divergence  $\langle -\nabla \cdot (qV) \rangle'$ , and its decomposed circulation  $\langle -(q\nabla \cdot V) \rangle'$  and moisture terms  $\langle -(V \cdot \nabla q) \rangle'$  during JJA(1) for El Niño. The pattern of  $\langle -\nabla \cdot (qV) \rangle'$  resembles the pattern of rainfall, showing the moisture flux divergence over the NWP, and at its south and north sides existing moisture flux convergence (Fig. 8a).

In addition,  $\langle -(q\nabla \cdot V) \rangle'$  plays a more dominant role than  $\langle -(V \cdot \nabla q) \rangle'$  in  $\langle -\nabla \cdot (qV) \rangle'$  (Fig. 8b, c). The moisture flux divergence over the NWP is further decomposed into six terms, which are shown in Figs. 9 and 10. The moisture flux divergence anomalies over the NWP are mainly attributed to the mean vertical gradient of humidity transported by anomalous vertical motion  $\langle -\omega' \partial_p \bar{q} \rangle'$ , emphasizing the influence of Kelvin wave-induced divergence (Fig. 6a). The contribution of rest terms is rather small.

With the disappearance of tropical Pacific SST anomalies, the Indian Ocean gradually plays a more important



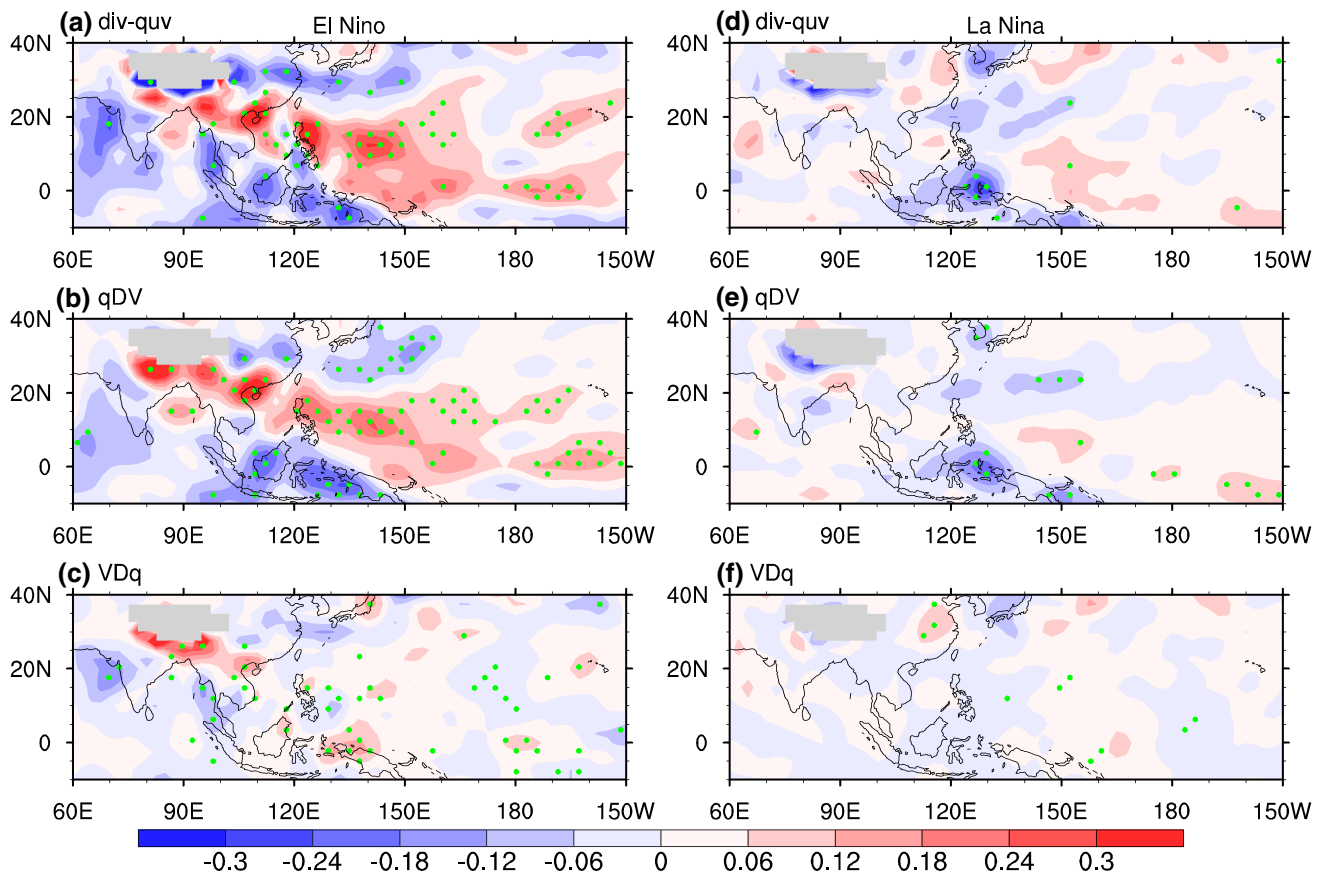


**Fig. 8** Composite anomalies of column-integrated moisture flux divergence ( $\langle -\nabla \cdot (qV) \rangle'$ ), and its decomposed circulation ( $\langle -(q\nabla \cdot V) \rangle'$ ) and moisture terms ( $\langle -(V \cdot \nabla q) \rangle'$ ) during JJA(1) for

El Niño (left panels **a–c**) and La Niña (right panels **d–f**). Dots indicate significant level reaches 90%

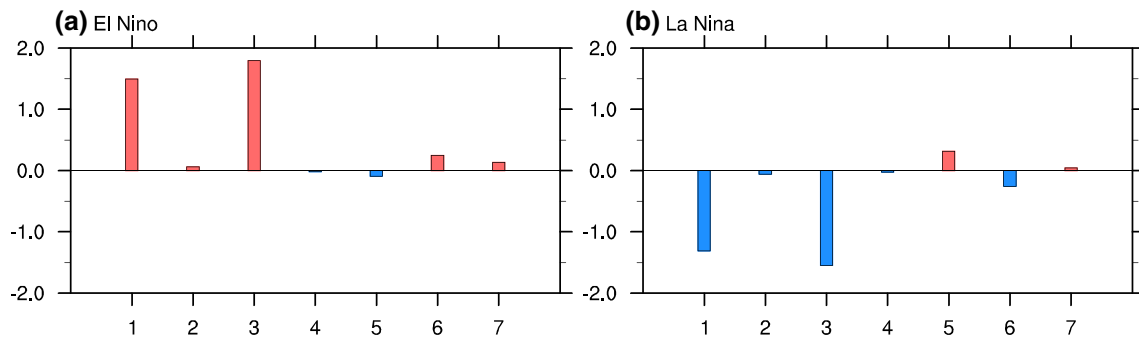


**Fig. 9** The regional mean moisture budget terms over the **a** NWP for El Niño and **b** MC&NWP for La Niña. No. 1–7 represent  $\langle -\nabla \cdot (qV) \rangle'$ ,  $\langle -\bar{\omega} \partial_p q \rangle'$ ,  $\langle -\omega' \partial_p \bar{q} \rangle'$ ,  $\langle -\omega' \partial_p q' \rangle'$ ,  $\langle -\bar{V} \cdot \nabla q' \rangle'$ ,  $\langle -V' \cdot \nabla \bar{q} \rangle'$  and  $\langle -V' \cdot \nabla q' \rangle'$ , respectively

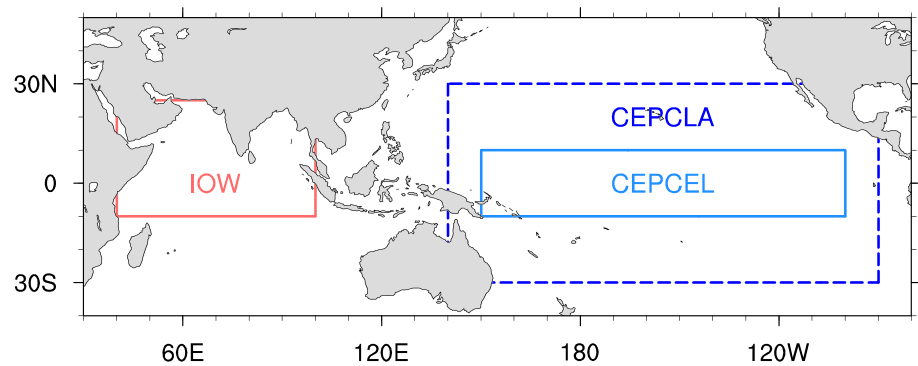
role (Yang et al. 2007, 2010; Wu et al. 2009a, 2010a; Xie et al. 2009). As a result, the tropical atmospheric waves and large-scale circulation anomalies could couple together and contribute to the development of NWPAC. Note that the equatorial CEP cooling during JJA(1) after the El Niño event also seems to contribute to the maintenance of NWPAC in some extent (Fan et al. 2013; Wang et al. 2013;

Xiang et al. 2013; Chen et al. 2015), which will be further examined by using AGCM.

#### 4.2 Rossby wave-induced convergence for La Niña

The La Niña related TT anomalies exists throughout the global tropical strip, and are weaker over the TIO than

**Fig. 10** Representation of the regions employed to force the simulations. *Red box* represents the region employed to force IOW, *blue box* represents the region employed to force CEPCEL, and *blue dashed box* represents the region employed to force CEPCLA in Table 2



CP (Fig. 6b). There are westward cold Rossby wave with significant westerly wind anomalies over the equatorial WP, indicating the response to equatorial CP negative rainfall anomalies (Fig. 3f). The lower level response of cold Rossby wave is the WP anticyclonic wind anomalies (Fig. 4f), which further cause the lower (upper) level convergence (divergence) over the MC and NWP (Fig. 7b, d). Then the resultant convergence leads to the enhanced convection there, inducing an anomalous cyclone as a Rossby wave response.

Figure 8d–f presents the composite anomalies of  $\langle -\nabla \cdot (qV)' \rangle$ ,  $\langle -(q\nabla \cdot V)' \rangle$  and  $\langle -(V \cdot \nabla q)' \rangle$  during JJA(1) for La Niña. For  $\langle -\nabla \cdot (qV)' \rangle$ , there are moisture flux divergence over the CP and moisture flux convergence over the MC and NWP (Fig. 8d), of which  $\langle -(q\nabla \cdot V)' \rangle$  account for a larger percentage than  $\langle -(V \cdot \nabla q)' \rangle$  (Fig. 8e, f). Furthermore,  $\langle -\omega' \partial_p \bar{q} \rangle$  is dominant in  $\langle -\nabla \cdot (qV)' \rangle$  over the MC&NWP, indicating the crucial effect of Rossby wave-induced convergence (Fig. 9b).

Besides, the equatorial easterly wind anomalies trigger the upwelling oceanic Kelvin wave and maintain the CEP cooling as the Bjerknes feedback (Okumura and Deser 2010; Okumura et al. 2011; Hu et al. 2013). Note that, the NWPC is mainly forced by equatorial CEP cooling, and the signal over the TIO is relatively weak (Figs. 6b, 7b, d). Unlike El Niño for which the TIO and equatorial CEP SST anomalies cooperate together to maintain the anomalous NWP circulation, the equatorial CEP cooling plays a more dominant role for La Niña. The mechanism for the maintenance of anomalous NWP circulation during ENSO decaying summer will be fully discussed by AGCM and LBM in the next section.

## 5 Model results

### 5.1 Solutions to the AGCM

The AGCM used is ECHAM6, the newest generation of AGCM developed by the Max Planck Institute for

Meteorology (Stevens et al. 2013). It is also the atmospheric component of the Earth System Model developed by the Max Planck Institute for Meteorology in Hamburg (MPI-ESM). In this study, a version with triangular truncation at zonal wavenumber 63 (T63; equivalent to 1.9° horizontal resolution) and 47 vertical levels extending to 0.01 hPa is used. A detailed description of ECHAM6 is given in Giorgetta et al. (2013).

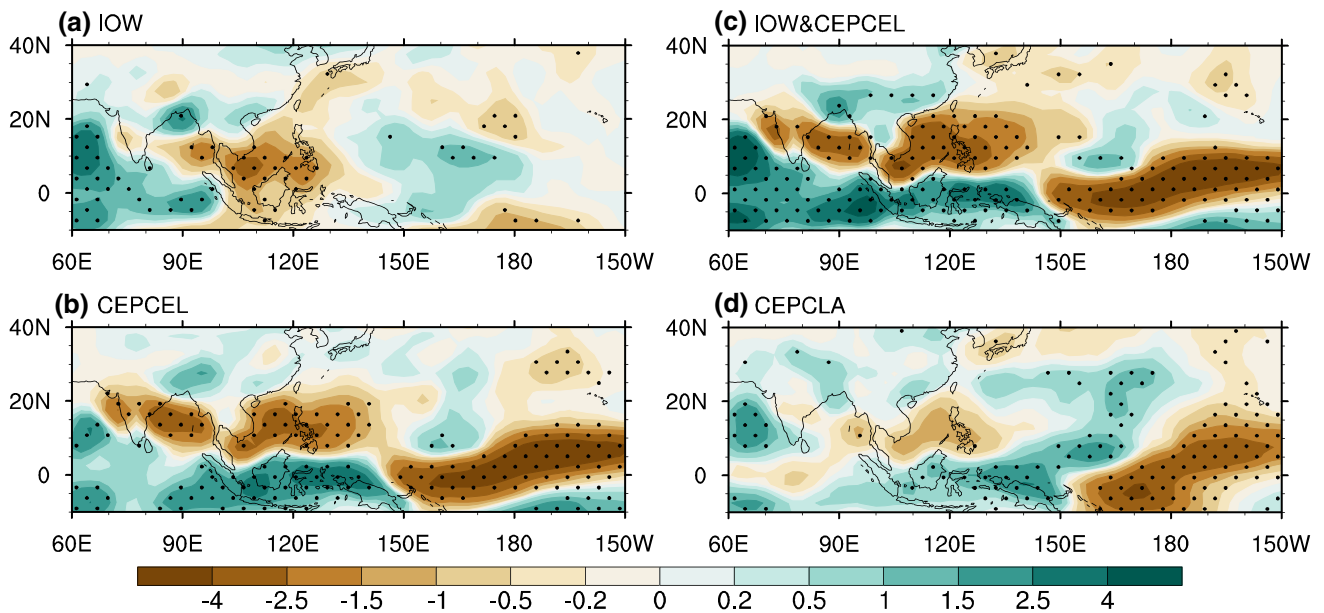
Five simulations using ECHAM6 model are conducted with different boundary conditions. In CTRL, the model is forced by the observed monthly climatology of SST and sea ice. For El Niño, a series of simulations are conducted to separate impacts of TIO warming and equatorial CEP cooling on NWPAC (i.e. IOW, CEPCEL and IOW&CEPCEL). For La Niña, additional composite negative SST anomalies are added over the CEP to identify the crucial influence of CEP cooling on NWPC (i.e. CEPCLA). The detailed information of simulations are referred to Table 2 and Fig. 10. In all experiments, the SST anomalies are kept constant in time and the model is integrated for 20 years. Thus, each simulation is equivalent to 20-member ensemble runs. Ensemble-mean results for JJA calculated as the departure from CTRL are analyzed.

#### 5.1.1 AGCM results for El Niño

The simulated rainfall and 850 hPa wind anomalies for IOW, CEPCEL and IOW&CEPCEL are presented in Figs. 11a–c and 12a–c, respectively. The observed characteristics are well reproduced in IOW&CEPCEL, although the simulations exist west shift (Figs. 11c, 12c). Also note that the CP dry anomalies is stronger than observation, and the wet anomalies on the north side of NWP dry anomalies are missing. Besides, the model results indicate that the NWPAC is maintained by a combined effect of the TIO warming and equatorial CEP cooling. Chen et al. (2015) have conducted the similar simulations by using CAM4, and found that the TIO warming is the main contribution in MAM(1) via Kelvin wave-induced divergence. However, the impact of the equatorial CEP cooling increases in

**Table 2** List of simulations: control run (CTRL), Indian Ocean warming run (IOW), CEP cooling run for El Niño (CEPCEL), IOW&CEPCEL run, and CEP cooling run for La Niña (CEPCLA)

| Simulation | SST forcing field   | Integration |
|------------|---|-------------|
| CTRL       | Global climatological SST   | 20          |
| IOW        | Added composite positive SST anomalies for El Niño to climatological SST over 10°S–25°N, 40–100°E (red box in Fig. 10) from June to August            | 20          |
| CEPCEL     | Added composite negative SST anomalies for El Niño to climatological SST over 10°S–10°N, 150°E–100°W (blue box in Fig. 10) from June to August        | 20          |
| IOW&CEPCEL | IOW + CEPCEL  | 20          |
| CEPCLA     | Added composite negative SST anomalies for La Niña to climatological SST over 30°S–30°N, 140°E–90°W (blue dashed box in Fig. 10) from March to August | 20          |

**Fig. 11** The simulated precipitation (mm) anomalies during JJA(1): **a** IOW minus CTRL, **b** CEPCEL minus CTRL, **c** IOW&CEPCEL minus CTRL. *Dots* indicate significant level reaches 90%

JJA(1). Here, the present study is consistent with their conclusions. Compared with TIO warming, the equatorial CEP cooling has a stronger impact on NWPAC during JJA(1), as shown in IOW and CEPCEL (Figs. 11a, b, 12a, b).

### 5.1.2 AGCM results for La Niña

Figures 11d and 12d show the difference of simulated rainfall and 850 hPa wind anomalies between CEPCLA and CTRL during JJA(1), respectively. Model results generally reproduce the observed characteristics. The SST anomalies over the CEP trigger the dry anomalies over the CP and wet anomalies with two centers over the MC and NWP (Fig. 11d), inducing the lower level anticyclonic and cyclonic wind anomalies over the CP and NWP as the Rossby wave response, respectively (Fig. 12d). Note that there exist some discrepancies in simulations, as the CP dry

anomalies is stronger, and the centers of MC&NWP wet anomalies and NWPC shift more eastward than observations. The unrealistic wet anomalies with anticyclonic wind anomalies are located over the west Indian Ocean, and stronger dry anomalies exist over the South China Sea than observation. Besides, previous studies have done detailed research on the mechanism for the maintenance of NWPAC during El Niño decaying summer (Yang et al. 2007, 2010; Wu et al. 2009a, 2010a; Xie et al. 2009). For these reasons, in next subsection, solutions to the LBM are considered to further examine the specific dynamic processes involved in how equatorial CEP cooling affects the NWPC.

### 5.2 Solutions to the LBM

The LBM described in Watanabe and Jin (2002) is used. The model is built upon atmospheric primitive equations

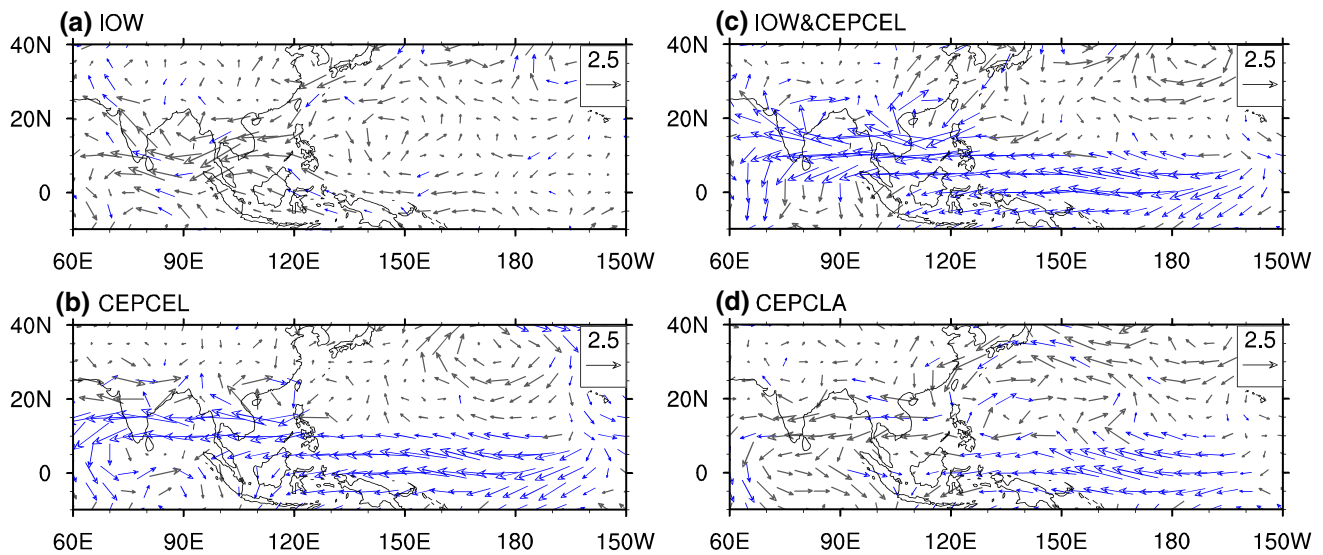


**Fig. 12** The simulated 850 hPa wind velocity ( $\text{m s}^{-1}$ ) anomalies during JJA(1): **a** IOW minus CTRL, **b** CEPCEL minus CTRL, **c** IOW&CEPCEL minus CTRL. Blue vectors indicate significant level reaches 90%

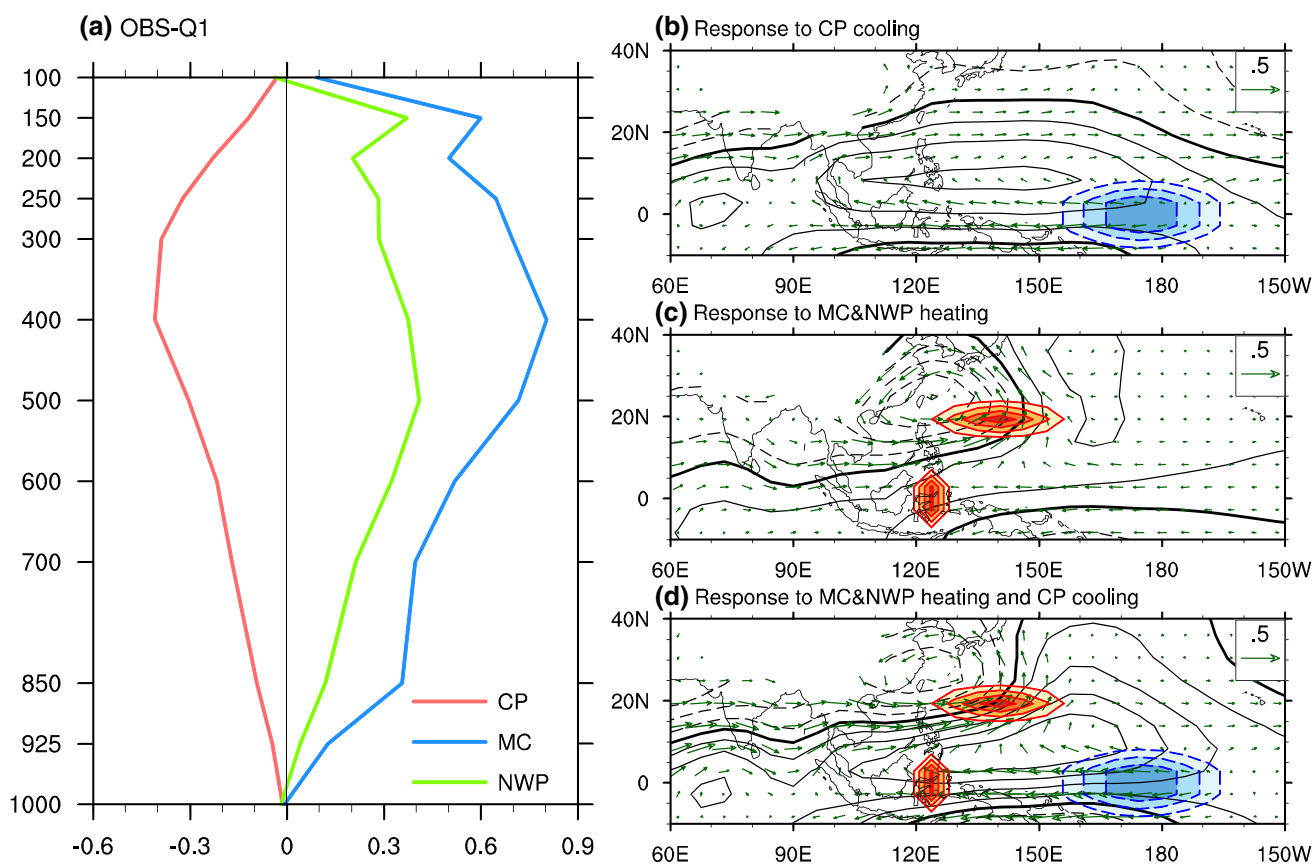
and has been widely used as a diagnostic tool for examining the steady linear response to idealized forcing (e.g., Annamalai et al. 2005; Xie et al. 2009; Zheng et al. 2010; Tao et al. 2014; Qu et al. 2015). Its horizontal resolution is T21, and it has 20 sigma levels in the vertical. The model employs horizontal and vertical diffusion, Rayleigh friction, and Newtonian damping. The latter two terms have a time scale of  $(1 \text{ day})^{-1}$  for  $\sigma \geq 0.9$  and  $\sigma \leq 0.03$ , while  $(30 \text{ day})^{-1}$  for  $0.03 < \sigma < 0.9$ . In this study, the dry version of the LBM is used to investigate the contribution of precipitation change to the circulation response. The horizontal shape of the heating is elliptical and the heating anomaly is imposed on summer (JJA) mean state from the NCEP–NCAR reanalysis. The vertical heating profile follows the gamma distribution, and the maximum heating is at  $\sigma = 0.45$ . The model is integrated for 50 days. The response reaches the equilibrium after 15 days, so the last 30 days are analyzed.

Figure 13a presents the vertical profile of diabatic heating anomalies averaged over the equatorial CP ( $10^{\circ}\text{S}$ – $10^{\circ}\text{N}$ ,  $150^{\circ}\text{E}$ – $160^{\circ}\text{W}$ ), MC ( $5^{\circ}\text{S}$ – $5^{\circ}\text{N}$ ,  $120^{\circ}$ – $130^{\circ}\text{E}$ ) and NWP ( $15^{\circ}$ – $25^{\circ}\text{N}$ ,  $120^{\circ}$ – $160^{\circ}\text{E}$ ). According to Yanai et al. (1973), the atmospheric apparent heat source  $Q_1$  is calculated to represent the total diabatic heating. The observed largest diabatic heating in the three regions are all located in 400–500 hPa (Fig. 13a), thus it is reasonable to put the maximum heating at  $\sigma = 0.45$  in the LBM. The heating rate is 1.6 K/day for the CP and NWP regions, and about 3 K  $\text{day}^{-1}$  for the MC region. Figure 10b–d shows the horizontal distribution of diabatic heating anomalies used to force the LBM, and the response of circulation anomalies to these heating. The negative diabatic heating in

Fig. 13b indicates the negative rainfall anomalies over the equatorial CP (center at  $0^{\circ}$  and  $175^{\circ}\text{E}$ ), with the zonal and meridional extent of  $25^{\circ}$  and  $10^{\circ}$ , respectively. To represent positive rainfall anomalies over the MC and NWP, idealized positive diabatic heating anomalies are imposed there (center at  $0^{\circ}$  and  $130^{\circ}\text{E}$ ,  $20^{\circ}$  and  $140^{\circ}\text{E}$ ), with the zonal extent of  $10^{\circ}$  and  $20^{\circ}$ , and the meridional extent of  $10^{\circ}$  and  $5^{\circ}$ , respectively (Fig. 13c).

As shown in Fig. 13b, the negative heating anomalies are imposed over the equatorial CP to simulate the dry anomalies induced by sea surface cooling. The equatorial CEP cooling-related negative rainfall anomalies over the CP trigger a pair of lower level off-equatorial anticyclones as the response of cold Rossby wave. On one hand, the easterly wind anomalies over the equatorial WP as a part of anomalous Walker circulation induce the wet anomalies over the MC (Fig. 3f). On the other hand, the southwesterly wind anomalies cause the moisture fluxes convergence over the NWP firstly, where the circulation term plays a more dominant role than moisture term (Figs. 8e, 9b). Then the moisture fluxes convergence leads to the wet anomalies over the NWP (Fig. 3f). As a result, the positive rainfall anomalies both over the MC and NWP are induced by the equatorial CEP cooling.

The response of circulation anomalies to MC&NWP heating is further examined in Fig. 13c. There are the cyclonic wind anomalies over the NWP and easterly wind anomalies over the equatorial WP. The wet anomalies over the MC and NWP cause the lower level NWPC and easterly wind anomalies as the response of warm Rossby and Kelvin wave, respectively. The equatorial easterly winds further induce the upwelling oceanic Kelvin wave, which



**Fig. 13** **a** Vertical profile of diabatic heating anomalies averaged over the equatorial CP (10°S–10°N, 150°E–160°W), MC (5°S–5°N, 120°–130°E) and NWP (15°–25°N, 120°–160°E) in observation. Vertical column-integrated diabatic heating anomalies imposed for **b** CP cooling (blue dashed contour and shaded CI = 0.2 K day<sup>-1</sup>),

**c** MC&NWP heating (red contour and shaded CI = 0.2 K day<sup>-1</sup>), **d** MC&NWP heating and CP cooling, and the response of 850 hPa wind velocity (vector m s<sup>-1</sup>) and stream function (contour m<sup>2</sup> s<sup>-1</sup>) to the heating anomalies

maintains the equatorial CEP cooling as the Bjerknes feedback, and even leads to the development of another La Niña. Several studies have reported the importance of zonal wind anomalies over the equatorial WP induced by the TIO SST anomalies in the phase transition of ENSO (Wu and Kirtman 2004; Annamalai et al. 2005; Kug et al. 2005; Kug and Kang 2006; Ohba and Ueda 2007). In present study, the equatorial easterly wind anomalies are important to the persistence of equatorial CEP cooling (Okumura and Deser 2010; Okumura et al. 2011; Hu et al. 2013).

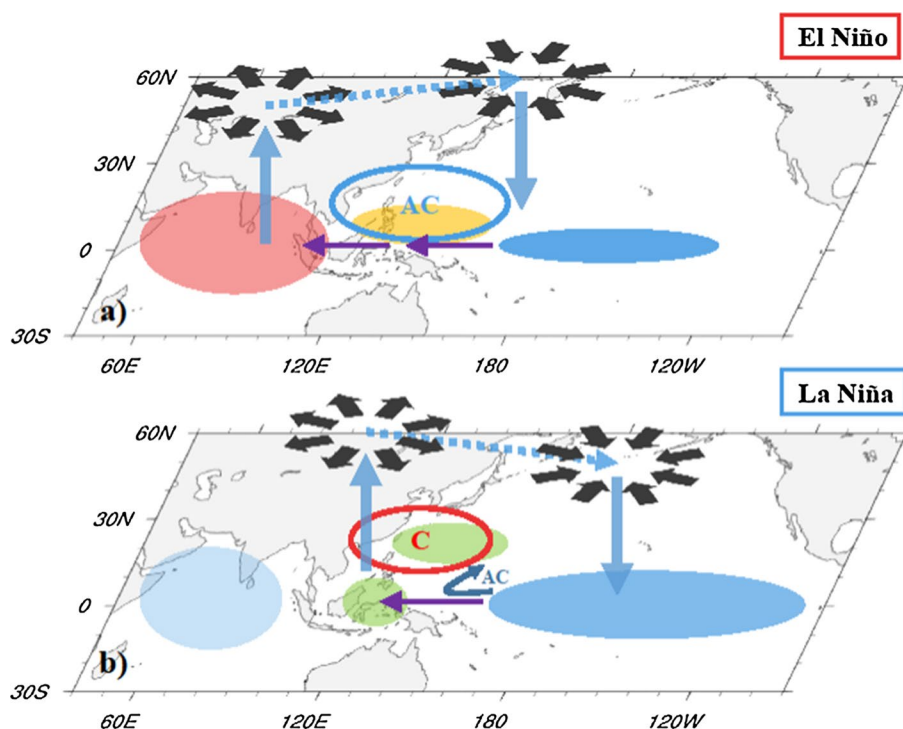
As shown in Fig. 13d, both positive and negative heating anomalies are imposed to investigate how the dry anomalies induced by sea surface cooling regulate the development of NWPC. There are anticyclonic and cyclonic wind anomalies over the WP and NWP, respectively. Compared to Fig. 13c, the NWPC shifts more northwestward, and its intensity weakens. The equatorial CEP cooling-related negative rainfall anomalies over the CP induce the anticyclonic wind anomalies as the response of cold Rossby wave, which regulate the location and intensity of NWPC.

Moreover, the equatorial easterly wind anomalies are strengthened, indicating the self-sustaining mechanism of equatorial CEP cooling.

## 6 Summary and discussion

Based on the results of statistical analysis and numerical experiments, the present study has revealed the asymmetric characteristics of summertime atmospheric circulation anomalies over the Indo-Pacific for El Niño and La Niña as well as the possible mechanism. During the summer when El Niño has dissipated, there are positive and negative SST anomalies over the TIO and equatorial CEP, respectively. Both observations and model results indicate that the NWPC is maintained by a combined effect of the TIO warming and equatorial CEP cooling. The TIO warming triggers the Matsuno-Gill (Matsuno 1966; Gill 1980) pattern with the warm tropospheric Kelvin wave eastward to the equatorial WP, which contributes to the development of

**Fig. 14** Schematic diagrams illustrate the main mechanisms involved in El Niño and La Niña. Red and blue shadings over the TIO and CEP represent SST anomalies. Black arrows represent the upper level convergence and divergence. Purple arrow represents lower level easterly wind anomalies forced by TIO warming for El Niño and equatorial CEP cooling for La Niña, respectively. The upward and downward blue arrows, purple arrow, and dashed blue arrow represent the large-scale circulation anomalies. Yellow and green shadings represent the negative and positive rainfall anomalies, respectively. ‘AC’ in blue circle represents the NWPAC. ‘C’ in red circle represents the NWPC. ‘AC’ with anticyclonic dark blue arrow represents the anticyclonic wind anomalies over the WP



NWPAC via the “capacitor effect” (Yang et al. 2007, 2010; Wu et al. 2009a; Xie et al. 2009). The impact of CEP cooling is by stimulating a Rossby wave response to its northwest (Fan et al. 2013; Wang et al. 2013; Xiang et al. 2013; Chen et al. 2015). Correspondingly, there are lower (upper) level convergence (divergence) over the TIO and divergence (convergence) over the NWP. As a result, the tropical atmospheric waves and large-scale circulation anomalies could couple together and contribute to the development of NWPAC. The whole processes for El Niño are illustrated by the schematic diagram in Fig. 14a.

The characteristics of SST, precipitation, circulation anomalies and tropical atmospheric waves for La Niña are different from El Niño. There still exists significant sea surface cooling over the equatorial CEP during the summer following La Niña event, forcing the zonal dipole rainfall anomalies. There are positive rainfall anomalies from the MC to NWP and negative rainfall anomalies over the equatorial CP. As the NWPAC for El Niño, an anomalous cyclone is located over the NWP, but its position shifts more northward. Besides, at the south flank of NWPC, there are anticyclonic wind anomalies over the WP. The response of tropical atmospheric waves and large-scale circulation indicates that the equatorial CEP cooling seems to play a more important role than TIO cooling in the maintenance of NWPC. To identify the crucial influence of CEP cooling, CEPCLA is designed with the composite SST anomalies added to climatological SST over the CEP to force an AGCM. The results of model generally reproduce the observed features.

Furthermore, the LBM is further used to reveal the detailed dynamic processes that equatorial CEP cooling influences the NWPC. The whole processes shown in Fig. 14b can be divided into two parts: First, the equatorial CEP cooling-related negative rainfall anomalies over the CP trigger anticyclonic wind anomalies over the WP as the response of cold Rossby wave. On one hand, the easterly wind anomalies over the equatorial WP as a part of anomalous Walker circulation induce the wet anomalies over the MC. On the other hand, the southwesterly wind anomalies cause the moisture fluxes convergence over the NWP, leading to the wet anomalies over the NWP. Thus, the positive rainfall anomalies over the MC and NWP are induced by the equatorial CEP cooling-related large-scale circulation anomalies. The lower level NWPC is triggered by the positive rainfall anomalies there as the response of warm Rossby wave, and the anticyclonic wind anomalies would regulate its location and intensity. Second, the MC&NWP positive rainfall anomalies further enhance equatorial easterly wind anomalies as the response of warm Kelvin wave. Thus, the equatorial CEP cooling-related zonal dipole rainfall anomalies are coupled with the equatorial easterly wind anomalies, which further trigger the upwelling oceanic Kelvin wave and maintain sea surface cooling as the Bjerknes feedback.

The anomalous NWP circulation for 1983 and 1984 La Niña events seem to have considerable strength compared with El Niño events (Fig. 5). Their relevant circulation patterns are checked, which are different from composite map

of El Niño (figures not shown). The NWPCs in 1983 and 1984 are slightly north than El Niño, and the anticyclonic wind anomalies over the WP cause moisture flux convergence over the MC&NWP and then the rainfall anomalies. The circulation discrepancy in these two events can be attributed to the SST pattern (figures not shown). For 1983 event, the warming persists over the NWP, and there still exists a positive feedback between local SST anomalies and NWPC. For 1984 event, the TIO cooling forces dry anomalies there, which seem to contribute the development of NWPC. Though the issues affecting the NWP circulation differs in 1983 and 1984 events, the key mechanism of the CEP cooling affecting the maintenance of NWPC still works.

The impacts of equatorial CEP cooling in El Niño and La Niña on the NWP circulation anomalies are different. For El Niño, the effect of equatorial CEP cooling is directly by stimulating a Rossby wave response to its northwest. For La Niña, however, the equatorial CEP cooling plays a dominant influence on the NWPC through the Rossby wave-induced convergence mechanism. The different impacts of the equatorial CEP cooling in El Niño and La Niña are due to their different distribution and duration. The El Niño related cooling show the significant SST anomalies over the equatorial CEP, which arise in JJA(1) (Fig. 2c). While the cooling in La Niña lasted from D(0)JF(1) to JJA(1) has a larger area and the maximum center is over the equatorial CP (Fig. 2f). Model results further demonstrate the different response of equatorial CEP cooling in El Niño and La Niña, as shown in Figs. 11b, d, 12b, d.

This study mainly focuses on the circulation anomalies over the NWP. However, precipitation is a good indicator describing the influence of the NWP circulation anomalies on EASM system. As shown in Fig. 3, anomalous NWP circulation-related summer rainfall patterns over East Asia in El Niño and La Niña are different. There are positive rainfall anomalies from the reaches of the Yangtze River to southern Japan for El Niño, indicating enhanced Meiyu/Baiu/Changma rainfall. The rainfall anomalies for La Niña do not show the rainband characteristic, and there are positive rainfall anomalies concentrated from 118° to 130°E, which are owing to that the center of anomalous NWP circulation is closer to the coast of East Asia than that of El Niño.

Besides, El Niño can be divided into several types, the central-Pacific and eastern-Pacific types (Ashok et al. 2007; Kao and Yu 2009; Kug et al. 2009), or according to its decay pace (Chowdary et al. 2016a, b), and the atmospheric response to different types of El Niño is also different. However, in the present study, we intend to reveal and contrast the different characteristics between El Niño and La Niña. The different types of El Niño are not considered for now, and this topic will be kept in our mind and further investigated in the future.

**Acknowledgements** We thank two anonymous reviewers as well as the editor for their useful comments. This work was supported by the National Natural Science Foundation of China (91337105, 41425019, 41275083 and 41205049) and the Public science and technology research funds projects of ocean (201505013).

## References

- Adler RF, Huffman GJ, Chang A, Ferraro R, Xie P-P, Janowiak J, Rudolf B, Schneider U, Curtis S, Bolvin D, Gruber A, Susskind J, Arkin P, Nelkin E (2003) The version-2 Global Precipitation Climatology Project (GPCP) monthly precipitation analysis (1979-present). *J Hydrometeorol* 4(6):1147–1167. doi:[10.1175/1525-7541\(2003\)004<1147:tvggpcp>2.0.co;2](https://doi.org/10.1175/1525-7541(2003)004<1147:tvggpcp>2.0.co;2)
- An S-I, Jin F-F (2004) Nonlinearity and asymmetry of ENSO\*. *J Clim* 17(12):2399–2412. doi:[10.1175/1520-0442\(2004\)017<2399:naao>2.0.co;2](https://doi.org/10.1175/1520-0442(2004)017<2399:naao>2.0.co;2)
- Annamalai H, Xie SP, McCreary JP, Murtugudde R (2005) Impact of Indian Ocean sea surface temperature on developing El Niño. *J Clim* 18(2):302–319. doi:[10.1175/jcli-3268.1](https://doi.org/10.1175/jcli-3268.1)
- Ashok K, Behera SK, Rao SA, Weng H, Yamagata T (2007) El Niño Modoki and its possible teleconnection. *J Geophys Res* 112(C11):C11007
- Burgers G, Stephenson DB (1999) The “normality” of El Niño. *Geophys Res Lett* 26(8):1027–1030. doi:[10.1029/1999gl900161](https://doi.org/10.1029/1999gl900161)
- Chang CP, Zhang Y, Li T (2000a) Interannual and interdecadal variations of the East Asian summer monsoon and tropical Pacific SSTs. Part I: roles of the subtropical ridge. *J Clim* 13(24):4310–4325. doi:[10.1175/1520-0442\(2000\)013<4310:iaivot>2.0.co;2](https://doi.org/10.1175/1520-0442(2000)013<4310:iaivot>2.0.co;2)
- Chang CP, Zhang Y, Li T (2000b) Interannual and interdecadal variations of the East Asian summer monsoon and tropical Pacific SSTs. Part II: meridional structure of the monsoon. *J Clim* 13(24):4326–4340. doi:[10.1175/1520-0442\(2000\)013<4326:iaivot>2.0.co;2](https://doi.org/10.1175/1520-0442(2000)013<4326:iaivot>2.0.co;2)
- Chen X, Zhou T (2014) Relative role of tropical SST forcing in the 1990s periodicity change of the Pacific-Japan pattern interannual variability. *Journal of Geophysical Research: Atmospheres* 119(23):JD022064. doi:[10.1002/2014jd022064](https://doi.org/10.1002/2014jd022064)
- Chen W, Feng J, Wu R (2012) Roles of ENSO and PDO in the link of the East Asian winter monsoon to the following summer monsoon. *J Clim* 26(2):622–635. doi:[10.1175/jcli-d-12-00021.1](https://doi.org/10.1175/jcli-d-12-00021.1)
- Chen Z, Wen Z, Wu R, Zhao P, Cao J (2014) Influence of two types of El Niños on the East Asian climate during boreal summer: a numerical study. *Clim Dyn* 43(1–2):469–481. doi:[10.1007/s00382-013-1943-1](https://doi.org/10.1007/s00382-013-1943-1)
- Chen Z, Wen Z, Wu R, Lin X, Wang J (2015) Relative importance of tropical SST anomalies in maintaining the Western North Pacific anomalous anticyclone during El Niño to La Niña transition years. *Clim Dyn*. doi:[10.1007/s00382-015-2630-1](https://doi.org/10.1007/s00382-015-2630-1)
- Chowdary JS, Harsha HS, Gnanaseelan C, Srinivas G, Parekh A, Pillai P, Naidu CV (2016a) Indian summer monsoon rainfall variability in response to differences in the decay phase of El Niño. *Clim Dyn*. doi:[10.1007/s00382-016-3233-1](https://doi.org/10.1007/s00382-016-3233-1)
- Chowdary JS, Parekh A, Kakatkar R, Gnanaseelan C, Srinivas G, Singh P, Roxy MK (2016b) Tropical Indian Ocean response to the decay phase of El Niño in a coupled model and associated changes in south and east-Asian summer monsoon circulation and rainfall. *Clim Dyn* 47(3):831–844. doi:[10.1007/s00382-015-2874-9](https://doi.org/10.1007/s00382-015-2874-9)
- Chung P-H, Sui C-H, Li T (2011) Interannual relationships between the tropical sea surface temperature and summertime subtropical anticyclone over the western North Pacific. *J Geophys Res Atmos* 116(D13):D13111. doi:[10.1029/2010jd015554](https://doi.org/10.1029/2010jd015554)
- Du Y, Xie SP, Huang G, Hu K (2009) Role of air–sea interaction in the long persistence of El Niño-induced North Indian Ocean warming. *J Clim* 22(8):2023–2038

- Fan L, Shin S-I, Liu Q, Liu Z (2013) Relative importance of tropical SST anomalies in forcing East Asian summer monsoon circulation. *Geophys Res Lett* 40(10):2471–2477. doi:[10.1002/grl.50494](https://doi.org/10.1002/grl.50494)
- Gill AE (1980) Some simple solutions for heat-induced tropical circulation. *Q J R Meteorol Soc* 106(449):447–462. doi:[10.1256/smsqj.44904](https://doi.org/10.1256/smsqj.44904)
- Giorgetta MA, Roeckner E, Mauritsen T, Bader J, Crueger T, Esch M, Rast S, Kornblueh L, Schmidt H, Kinne S, Hohenegger C, Möbis B, Krismer T, Wieners K-H, Stevens B (2013) The atmospheric general circulation model ECHAM6—model description. *Berichte zur Erdsystemforschung/Max-Planck-Institut für Meteorologie*. Max-Planck-Institut für Meteorologie, Hamburg. doi:[10.17617/2.1810480](https://doi.org/10.17617/2.1810480)
- Hoerling MP, Kumar A, Zhong M (1997) El Niño, La Niña, and the nonlinearity of their teleconnections. *J Clim* 10(8):1769–1786. doi:[10.1175/1520-0442\(1997\)010<1769:enolna>2.0.co;2](https://doi.org/10.1175/1520-0442(1997)010<1769:enolna>2.0.co;2)
- Hu Z-Z, Kumar A, Xue Y, Jha B (2013) Why were some La Niñas followed by another La Niña? *Clim Dyn*. doi:[10.1007/s00382-013-1917-3](https://doi.org/10.1007/s00382-013-1917-3)
- Huang RH, Sun FY (1992) Impacts of the tropical western Pacific on the East-Asian summer monsoon. *J Meteorol Soc Jpn* 70(1B):243–256
- Huang R, Wu Y (1989) The influence of ENSO on the summer climate change in China and its mechanism. *Adv Atmos Sci* 6(1):21–32. doi:[10.1007/bf02656915](https://doi.org/10.1007/bf02656915)
- Huang G, Hu KM, Xie SP (2010) Strengthening of tropical Indian Ocean teleconnection to the Northwest Pacific since the mid-1970s: an atmospheric GCM study. *J Clim* 23(19):5294–5304. doi:[10.1175/2010jcli3577.1](https://doi.org/10.1175/2010jcli3577.1)
- Jin F-F, An S-I, Timmermann A, Zhao J (2003) Strong El Niño events and nonlinear dynamical heating. *Geophys Res Lett* 30(3):1120. doi:[10.1029/2002gl016356](https://doi.org/10.1029/2002gl016356)
- Kalnay E, Kanamitsu M, Kistler R, Collins W, Deaven D, Gandin L, Iredell M, Saha S, White G, Woollen J, Zhu Y, Chelliah M, Ebisuzaki W, Higgins W, Janowiak J, Mo KC, Ropelewski C, Wang J, Leetmaa A, Reynolds R, Jenne R, Joseph D (1996) The NCEP/NCAR 40-year reanalysis project. *Bull Am Meteorol Soc* 77(3):437–471. doi:[10.1175/1520-0477\(1996\)077<0437:tnypr>2.0.co;2](https://doi.org/10.1175/1520-0477(1996)077<0437:tnypr>2.0.co;2)
- Kang I-S, Kug J-S (2002) El Niño and La Niña sea surface temperature anomalies: asymmetry characteristics associated with their wind stress anomalies. *J Geophys Res Atmos* 107(D19):4372. doi:[10.1029/2001jd000393](https://doi.org/10.1029/2001jd000393)
- Kao HY, Yu JY (2009) Contrasting eastern-Pacific and central-Pacific types of ENSO. *J Clim* 22(3):615–632
- Karori MA, Li JP, Jin FF (2013) The asymmetric influence of the two types of El Niño and La Niña on summer rainfall over Southeast China. *J Clim* 26(13):4567–4582. doi:[10.1175/jcli-d-12-00324.1](https://doi.org/10.1175/jcli-d-12-00324.1)
- Kessler WS (2002) Is ENSO a cycle or a series of events? *Geophys Res Lett* 29(23):2125. doi:[10.1029/2002gl015924](https://doi.org/10.1029/2002gl015924)
- Klein SA, Soden BJ, Lau N-C (1999) Remote sea surface temperature variations during ENSO: evidence for a tropical atmospheric bridge. *J Clim* 12(4):917–932. doi:[10.1175/1520-0442\(1999\)012<0917:rsstvd>2.0.co;2](https://doi.org/10.1175/1520-0442(1999)012<0917:rsstvd>2.0.co;2)
- Kug JS, Kang IS (2006) Interactive feedback between ENSO and the Indian Ocean. *J Clim* 19(9):1784–1801. doi:[10.1175/jcli3660.1](https://doi.org/10.1175/jcli3660.1)
- Kug JS, An SI, Jin FF, Kang IS (2005) Preconditions for El Niño and La Niña onsets and their relation to the Indian Ocean. *Geophys Res Lett*. doi:[10.1029/2004gl021674](https://doi.org/10.1029/2004gl021674)
- Kug J-S, Jin F-F, An S-I (2009) Two types of El Niño events: cold tongue El Niño and warm pool El Niño. *J Clim* 22(6):1499–1515. doi:[10.1175/2008jcli2624.1](https://doi.org/10.1175/2008jcli2624.1)
- Larkin NK, Harrison DE (2002) ENSO warm (El Niño) and cold (La Niña) event life cycles: ocean surface anomaly patterns, their symmetries, asymmetries, and implications. *J Clim* 15(10):1118–1140. doi:[10.1175/1520-0442\(2002\)015<1118:ewenao>2.0.co;2](https://doi.org/10.1175/1520-0442(2002)015<1118:ewenao>2.0.co;2)
- Lau NC, Nath MJ (1996) The role of the “atmospheric bridge” in linking tropical Pacific ENSO events to extratropical SST anomalies. *J Clim* 9:2036–2057
- Lu R, Lu S (2014) Asymmetric relationship between Indian Ocean SST and the Western North Pacific summer monsoon. *J Clim* 28(4):1383–1395. doi:[10.1175/jcli-d-14-00289.1](https://doi.org/10.1175/jcli-d-14-00289.1)
- Matsuno T (1966) Quasi-geostrophic motions in the equatorial area. *J Meteorol Soc Jpn* 44(1):25–43
- McPhaden MJ, Zhang X (2009) Asymmetry in zonal phase propagation of ENSO sea surface temperature anomalies. *Geophys Res Lett* 36(13):L13703. doi:[10.1029/2009gl038774](https://doi.org/10.1029/2009gl038774)
- Ohba M, Ueda H (2007) An impact of SST anomalies in the Indian Ocean in acceleration of the El Niño to La Niña transition. *J Meteorol Soci Jpn Ser II* 85(3):335–348. doi:[10.2151/jmsj.85.335](https://doi.org/10.2151/jmsj.85.335)
- Okumura YM, Deser C (2010) Asymmetry in the duration of El Niño and La Niña. *J Clim* 23(21):5826–5843. doi:[10.1175/2010jcli3592.1](https://doi.org/10.1175/2010jcli3592.1)
- Okumura YM, Ohba M, Deser C, Ueda H (2011) A proposed mechanism for the asymmetric duration of El Niño and La Niña. *J Clim* 24(15):3822–3829. doi:[10.1175/2011jcli3999.1](https://doi.org/10.1175/2011jcli3999.1)
- Qu X, Huang G, Hu K, Xie S-P, Du Y, Zheng X-T, Liu L (2015) Equatorward shift of the South Asian high in response to anthropogenic forcing. *Theor Appl Climatol* 119(1–2):113–122. doi:[10.1007/s00704-014-1095-1](https://doi.org/10.1007/s00704-014-1095-1)
- Rayner NA, Parker DE, Horton EB, Folland CK, Alexander LV, Rowell DP, Kent EC, Kaplan A (2003) Global analyses of sea surface temperature, sea ice, and night marine air temperature since the late nineteenth century. *J Geophys Res Atmos* 108(D14):4407. doi:[10.1029/2002jd002670](https://doi.org/10.1029/2002jd002670)
- Stevens B, Giorgetta M, Esch M, Mauritsen T, Crueger T, Rast S, Salzmann M, Schmidt H, Bader J, Block K, Brokopf R, Fast I, Kinne S, Kornblueh L, Lohmann U, Pincus R, Reichler T, Roeckner E (2013) Atmospheric component of the MPI-M Earth System Model: ECHAM6. *J Adv Model Earth Syst* 5(2):146–172. doi:[10.1002/jame.20015](https://doi.org/10.1002/jame.20015)
- Su J, Zhang R, Li T, Rong X, Kug JS, Hong C-C (2010) Causes of the El Niño and La Niña amplitude asymmetry in the equatorial eastern Pacific. *J Clim* 23(3):605–617. doi:[10.1175/2009jcli2894.1](https://doi.org/10.1175/2009jcli2894.1)
- Tao W, Huang G, Hu K, Qu X, Wen G, Gong Y (2014) Different influences of two types of El Niños on the Indian Ocean SST variations. *Theor Appl Climatol* 117(3–4):475–484. doi:[10.1007/s00704-013-1022-x](https://doi.org/10.1007/s00704-013-1022-x)
- Tao W, Huang G, Hu K, Gong H, Wen G, Liu L (2015) A study of biases in simulation of the Indian Ocean basin mode and its capacitor effect in CMIP3/CMIP5 models. *Clim Dyn* 46(1):205–226. doi:[10.1007/s00382-015-2579-0](https://doi.org/10.1007/s00382-015-2579-0)
- Trenberth KE, Branstator GW, Karoly D, Kumar A, Lau N-C, Ropelewski C (1998) Progress during TOGA in understanding and modeling global teleconnections associated with tropical sea surface temperatures. *J Geophys Res Oceans* 103(C7):14291–14324. doi:[10.1029/97jc01444](https://doi.org/10.1029/97jc01444)
- Wang B (1995) Interdecadal changes in El Niño onset in the last four decades. *J Clim* 8(2):267–285. doi:[10.1175/1520-0442\(1995\)008<0267:icienio>2.0.co;2](https://doi.org/10.1175/1520-0442(1995)008<0267:icienio>2.0.co;2)
- Wang B, Fan Z (1999) Choice of South Asian summer monsoon indices. *Bull Am Meteorol Soc* 80(4):629–638. doi:[10.1175/1520-0477\(1999\)080<0629:cosasm>2.0.co;2](https://doi.org/10.1175/1520-0477(1999)080<0629:cosasm>2.0.co;2)
- Wang L, Wu R (2012) In-phase transition from the winter monsoon to the summer monsoon over East Asia: role of the Indian Ocean. *J Geophys Res Atmos* 117(D11):D11112. doi:[10.1029/2011jd017509](https://doi.org/10.1029/2011jd017509)
- Wang B, Zhang Q (2002) Pacific-east Asian teleconnection. Part II: how the Philippine Sea anomalous anticyclone is established during El Niño development. *J Clim* 15(22):3252–3265. doi:[10.1175/1520-0442\(2002\)015<3252:peatpi>2.0.co;2](https://doi.org/10.1175/1520-0442(2002)015<3252:peatpi>2.0.co;2)



- Wang B, Wu RG, Fu XH (2000) Pacific-East Asian teleconnection: how does ENSO affect East Asian climate? *J Clim* 13(9):1517–1536. doi:[10.1175/1520-0442\(2000\)013<1517:peathd>2.0.co;2](https://doi.org/10.1175/1520-0442(2000)013<1517:peathd>2.0.co;2)
- Wang B, Yang J, Zhou T (2008) Interdecadal changes in the major modes of Asian-Australian monsoon variability: strengthening relationship with ENSO since the late 1970s\*. *J Clim* 21(8):1771–1789. doi:[10.1175/2007jcli1981.1](https://doi.org/10.1175/2007jcli1981.1)
- Wang B, Xiang B, Lee J-Y (2013) Subtropical high predictability establishes a promising way for monsoon and tropical storm predictions. *Proc Natl Acad Sci* 110(8):2718–2722. doi:[10.1073/pnas.1214626110](https://doi.org/10.1073/pnas.1214626110)
- Watanabe M, Jin F (2002) Role of Indian Ocean warming in the development of Philippine Sea anticyclone during ENSO. *Geophys Res Lett* 29(10):1478
- Webster PJ, Magaña VO, Palmer TN, Shukla J, Tomas RA, Yanai M, Yasunari T (1998) Monsoons: processes, predictability, and the prospects for prediction. *J Geophys Res Oceans* 103(C7):14451–14510. doi:[10.1029/97jc02719](https://doi.org/10.1029/97jc02719)
- Wu R, Kirtman BP (2004) Understanding the impacts of the Indian Ocean on ENSO variability in a coupled GCM. *J Clim* 17(20):4019–4031. doi:[10.1175/1520-0442\(2004\)017<4019:utio>2.0.co;2](https://doi.org/10.1175/1520-0442(2004)017<4019:utio>2.0.co;2)
- Wu RG, Hu ZZ, Kirtman BP (2003) Evolution of ENSO-related rainfall anomalies in East Asia. *J Clim* 16(22):3742–3758. doi:[10.1175/1520-0442\(2003\)016<3742:eoerai>2.0.co;2](https://doi.org/10.1175/1520-0442(2003)016<3742:eoerai>2.0.co;2)
- Wu R, Kirtman BP, Krishnamurthy V (2008) An asymmetric mode of tropical Indian Ocean rainfall variability in boreal spring. *J Geophys Res Atmos* 113(D5):D05104. doi:[10.1029/2007jd009316](https://doi.org/10.1029/2007jd009316)
- Wu B, Zhou T, Li T (2009a) Seasonally evolving dominant interannual variability modes of East Asian climate\*. *J Clim* 22(11):2992–3005. doi:[10.1175/2008jcli2710.1](https://doi.org/10.1175/2008jcli2710.1)
- Wu R, Wen Z, Yang S, Li Y (2009b) An interdecadal change in southern China summer rainfall around 1992/93. *J Clim* 23(9):2389–2403. doi:[10.1175/2009jcli3336.1](https://doi.org/10.1175/2009jcli3336.1)
- Wu B, Li T, Zhou T (2010a) Relative contributions of the Indian Ocean and local SST anomalies to the maintenance of the Western North Pacific anomalous anticyclone during the El Niño decaying summer\*. *J Clim* 23(11):2974–2986. doi:[10.1175/2010jcli3300.1](https://doi.org/10.1175/2010jcli3300.1)
- Wu B, Li T, Zhou TJ (2010b) Asymmetry of atmospheric circulation anomalies over the Western North Pacific between El Niño and La Niña. *J Clim* 23(18):4807–4822. doi:[10.1175/2010jcli3222.1](https://doi.org/10.1175/2010jcli3222.1)
- Wu R, Yang S, Wen Z, Huang G, Hu K (2012) Interdecadal change in the relationship of southern China summer rainfall with tropical Indo-Pacific SST. *Theor Appl Climatol* 108(1–2):119–133. doi:[10.1007/s00704-011-0519-4](https://doi.org/10.1007/s00704-011-0519-4)
- Xiang B, Wang B, Yu W, Xu S (2013) How can anomalous western North Pacific Subtropical High intensify in late summer? *Geophys Res Lett* 40(10):2349–2354. doi:[10.1002/grl.50431](https://doi.org/10.1002/grl.50431)
- Xie SP, Annamalai H, Schott FA, McCreary JP Jr (2002) Structure and mechanisms of south Indian Ocean climate variability. *J Clim* 15(8):864–878
- Xie SP, Hu K, Hafner J, Tokinaga H, Du Y, Huang G, Sampe T (2009) Indian Ocean capacitor effect on Indo-western Pacific climate during the summer following El Niño. *J Clim* 22(3):730–747
- Xie SP, Du Y, Huang G, Zheng XT, Tokinaga H, Hu KM, Liu QY (2010) Decadal shift in El Niño influences on Indo-Western Pacific and East Asian climate in the 1970s. *J Clim* 23(12):3352–3368. doi:[10.1175/2010jcli3429.1](https://doi.org/10.1175/2010jcli3429.1)
- Yanai M, Esbensen S, Chu J-H (1973) Determination of bulk properties of tropical cloud clusters from large-scale heat and moisture budgets. *J Atmos Sci* 30(4):611–627. doi:[10.1175/1520-0469\(1973\)030<0611:DOBPOT>2.0.CO;2](https://doi.org/10.1175/1520-0469(1973)030<0611:DOBPOT>2.0.CO;2)
- Yang J, Liu Q, Xie S, Liu Z, Wu L (2007) Impact of the Indian Ocean SST basin mode on the Asian summer monsoon. *Geophys Res Lett* 34(2):L02708. doi:[10.1029/2006gl028571](https://doi.org/10.1029/2006gl028571)
- Yang J, Liu Q, Liu Z (2010) Linking observations of the Asian monsoon to the Indian Ocean SST: possible roles of Indian Ocean Basin mode and dipole mode. *J Clim* 23(21):5889–5902. doi:[10.1175/2010jcli2962.1](https://doi.org/10.1175/2010jcli2962.1)
- Zhang RH, Sumi A, Kimoto M (1996) Impact of El Niño on the East Asian monsoon: a diagnostic study of the '86/87 and '91/92 events. *J Meteorol Soc Jpn* 74(1):49–62
- Zhang R, Li T, Wen M, Liu L (2014) Role of intraseasonal oscillation in asymmetric impacts of El Niño and La Niña on the rainfall over southern China in boreal winter. *Clim Dyn*. doi:[10.1007/s00382-014-2207-4](https://doi.org/10.1007/s00382-014-2207-4)
- Zheng X-T, Xie S-P, Vecchi GA, Liu Q, Hafner J (2010) Indian Ocean dipole response to global warming: analysis of ocean-atmospheric feedbacks in a coupled model\*. *J Clim* 23(5):1240–1253. doi:[10.1175/2009jcli3326.1](https://doi.org/10.1175/2009jcli3326.1)